JACS
JOURNAL OF THE AMERICAN CHEMICAL SOCIETY
Article
pubs.acs.org/JACS

Single-Handed Helical Wrapping of Single-Walled Carbon Nanotubes by Chiral, Ionic, Semiconducting Polymers

Pravas Deria,[†] Christopher D. Von Bargen,[‡] Jean-Hubert Olivier,[†] Amar S. Kumbhar,[§] Jeffery G. Saven,*[,‡] and Michael J. Therien*[,†]

[†]Department of Chemistry, French Family Science Center, Duke University, Durham, North Carolina 27708, United States
[‡]Department of Chemistry, University of Pennsylvania, Philadelphia, Pennsylvania 19104, United States
[§]Chapel Hill Analytical & Nanofabrication Laboratory, University of North Carolina−Chapel Hill, Chapel Hill, North Carolina 27599, United States

Supporting Information

ABSTRACT: We establish the requisite design for arylene-ethynylene polymers that give rise to single-handed helical wrapping of single-walled carbon nanotubes (SWNTs). Highly charged semiconducting polymers that utilize either an (*R*)- or (*S*)-1,1′-bi-2-naphthol component in their respective conjugated backbones manifest HRTEM and AFM images of single-chain-wrapped SWNTs that reveal significant preferences for the anticipated helical wrapping handedness; statistical analysis of these images, however, indicates that ∼20% of the helical structures are formed with the "unexpected" handedness. CD spectroscopic data, coupled with TDDFT-based computational studies that correlate the spectral signatures of semiconducting polymer-wrapped SWNT assemblies with the structural properties of the chiral 1,1′-binaphthyl unit, suggest strongly that two distinct binaphthalene SWNT binding modes, *cisoid-facial* and *cisoid-side*, are possible for these polymers, with the latter mode responsible for inversion of helical chirality and the population of polymer-SWNT superstructures that feature the unexpected polymer helical wrapping chirality at the nanotube surface. Analogous aryleneethynylene polymers were synthesized that feature a 2,2′-(1,3-benzyloxy)-*bridged* (b)-1,1′-bi-2-naphthol unit: this 1,1′-bi-2-naphthol derivative is characterized by a *bridging* 2,2′−1,3 benzyloxy tether that restricts the torsional angle between the two naphthalene subunits along its C1−C1′ chirality axis to larger, oblique angles that facilitate more extensive van der Waals contact of the naphthyl subunits with the nanotube. Similar microscopic, spectroscopic, and computational studies determine that chiral polymers based on conformationally restricted *transoid* binaphthyl units direct preferential *facial* binding of the polymer with the SWNT and thereby guarantee helically wrapped polymer-nanotube superstructures of fixed helical chirality. Molecular dynamics simulations provide an integrated picture tying together the global helical superstructure and conformational properties of the binaphthyl units: a robust, persistent helical handedness is preferred for the conformationally restricted *transoid* binaphthalene polymer. Further examples of similar semiconducting polymer-SWNT superstructures are reported that demonstrate that the combination of single-handed helical wrapping and electronic structural modification of the conjugated polymer motif opens up new opportunities for engineering the electro-optic functionality of nanoscale objects.

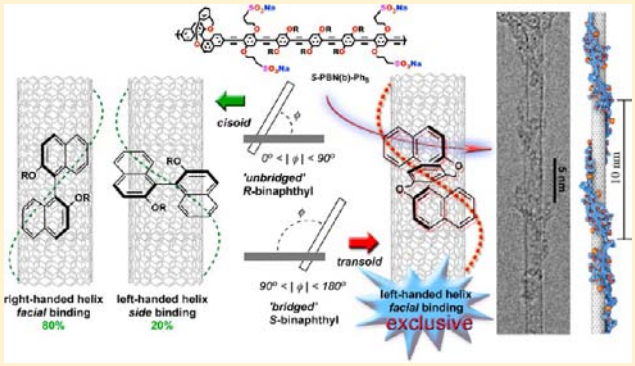

INTRODUCTION

The helical chirality of biological macromolecules such as DNA[1] and various synthetically designed organic[2] and organometallic[3] superstructures have played prominent roles in the development of liquid crystalline,[2b,4] optoelectronic,[2a,5] and spintronic[6] materials. For these designed helical superstructures, both covalent polymerization[2a−c,7] and self-assembly[5,8] of various chiral[5,8a,c,9] and achiral[8a,d−g,9b,10] units define commonly utilized synthetic strategies; helically chiral structures that possess electronic, electro-optical, nonlinear optical, or spintronic utility typically feature polarizable, hyperpolarizable, or low band gap building blocks that provide such functionality.[5,7,8e,g,11]

It is worth noting that a wide range of nanoscale structures have established semiconducting or conducting properties;[12] such nanoscale objects, if integrated into hybrid materials that engender helical chirality, offer the possibility to evolve entirely new classes of optoelectronic and spintronic materials. Among the semiconducting nanomaterials, certain types of single-walled carbon nanotubes (SWNTs)[13] are known to possess intrinsic helical chirality ($n \neq m$; $m \neq 0$);[14] combined with their established electro-optic properties,[13c,15] tunable valence and conduction bands, and high aspect ratio, semiconducting

Received: August 14, 2013
Published: September 26, 2013

dx.doi.org/10.1021/ja408430v | J. Am. Chem. Soc. 2013, 135, 16220−16234

Chart 1. Ionic Aryleneethynylene Polymers Based on 1,1′-Bi-2-naphthol Derivatives

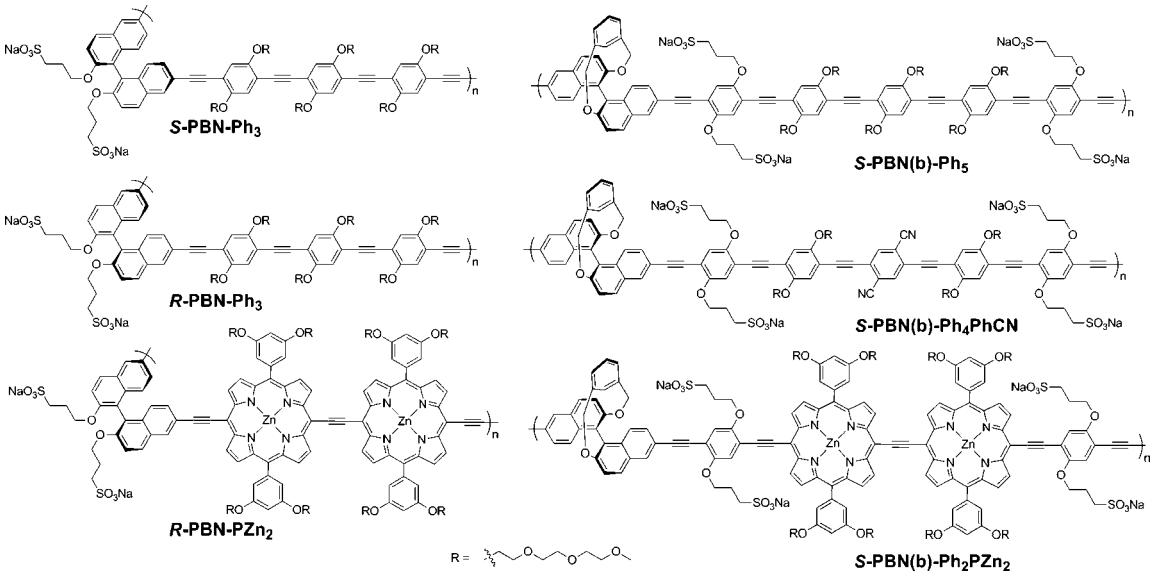

SWNTs define a particularly interesting nanoscale platform for integration into hybrid nanomaterials that also exploit helically chiral semiconducting polymers.

While chiral biological polymers such as DNA[16] and β-1,3-glucans[17] have been established to helically wrap and individualize SWNTs with well-defined periodicities, it is important to underscore that the building blocks of these polymers possess limited absorptive oscillator strength and frontier orbital energy levels far removed from the valence and conduction band energies of semiconducting SWNTs, making them less than ideal for developing hybrid nanomaterials for optoelectronics and spintronics that exploit helical chirality. Furthermore, in this regard, it is worth noting as well that although Brus has shown that a polynucleotide $d(GT)_{20}$-wrapped racemic [(6,5) SWNT] sample manifests induced circular dichroism (ICD) for the nanotube E_{22} and E_{11} transitions,[18] no evidence exists that establishes any correlation of the observed ICD signals with the handedness of helical superstructures formed via DNA wrapping on the SWNT surface; high-resolution AFM data that show both right- and left-handed helical SWNT wrapping by this polynucleotide indicate that the ICD likely stems from the interaction of the optically active electronic transition dipole moments associated with SWNTs and the chiral deoxyribose bases and is not correlated with the helical chirality of the DNA superstructure that wraps the SWNTs.[19] To date, there exists no general method to control the handedness of the helically wrapped superstructure in constructs comprising an individual polymer and SWNT.

Previous work from our group has demonstrated that linear, conjugated, highly charged poly[*p*-{2,5-bis(3-propoxysulfonicacidsodium salt)}phenylene]ethynylene (**PPES**) and poly[1,5-bis(3-propoxysulfonic acid sodium salt)-2,6-naphthylene]-ethynylene (**PNES**) exfoliate, individualize, and disperse SWNTs via a single chain helical wrapping mechanism.[20] **PPES** and **PNES** yield robust, helical superstructures wherein the polymer remains adhered to the SWNT in a variety of aqueous and organic solvents; such structures are stabilized by extensive van der Waals contact between the aryleneethynylene units and SWNT. **PNES**, used in combination with a suitable phase transfer agent, provides individualized, noncovalently modified SWNTs (**PNES-SWNTs**) of fixed morphology that retain established nanotube semiconducting and conducting properties, in a wide range of dielectric media.[20b,21] These **PNES-SWNTs** do not exhibit polymer dewrapping and SWNT precipitation in organic solvents; DMSO-, DMF-, and MeOH-solubilized **PNES-SWNTs** have been shown to persist in solution over time periods that exceed at least several months. Microscopic characterization data of **PNES-SWNTs** reveal a self-assembled superstructure in which a PNES monolayer helically wraps the nanotube surface with periodic and constant morphology (helix pitch length = 10 ± 2 nm);[20b] statistical analysis of TEM data obtained for such samples demonstrates equal numbers of right- and left-handed helically wrapped **PNES-SWNTs**. Like all other polymer-wrapped SWNT systems, PNES wraps SWNTs with no observed preference for helical chirality in its superstructure.

In this study, we exploit the axial chirality of the 1,1′-binaphthalene moiety to rigorously control the helical handedness of single chain, highly charged semiconducting polymers related to PNES that wrap SWNTs. Herein we (i) establish the requisite design criteria for enantiopure 1,1′-bi-2-naphthol moieties that are incorporated into the backbones of aryleneethynylene polymers in order to give rise to single-handed helical wrapping of SWNTs, (ii) analyze experimental CD spectroscopic data using TDDFT-based computational methods to correlate the spectral signatures of semiconducting polymer-wrapped SWNT assemblies with the structural properties of the chiral 1,1′-binaphthyl unit, (iii) provide a molecularly detailed perspective not accessible with experimental methods using molecular dynamics (MD) simulations, and (iv) demonstrate that electronic structural modification of conjugated polymer motifs that provide single-handed helical SWNT wrapping open up new opportunities for engineering the electro-optic functionality of nanoscale objects.

EXPERIMENTAL SECTION

Materials. Synthetic procedures and characterization data for monomeric and polymeric compounds are given in the Supporting Information. The M_n values of the aryleneethynylene polymers ***R*-PBN-Ph$_3$**, ***S*-PBN-Ph$_3$**, ***R*-PBN-PZn$_2$**, ***S*-PBN(b)-Ph$_5$**, ***S*-PBN(b)-Ph$_4$PhCN**, and ***S*-PBN(b)-Ph$_2$PZn$_2$** (Chart 1; Supplementary Figure

dx.doi.org/10.1021/ja408430v | J. Am. Chem. Soc. 2013, 135, 16220−16234

S5) were determined to be, respectively, ~21.3, 21.3, 21.6, 20.78, 14.5, and 20.1 kD by gel permeation chromatography (GPC); polymers ***R*-PBN-Ph$_3$**, ***S*-PBN-Ph$_3$**, ***R*-PBN-PZn$_2$**, ***S*-PBN(b)-Ph$_5$**, ***S*-PBN(b)-Ph$_4$PhCN**, and ***S*-PBN(b)-Ph$_2$PZn$_2$** thus possess correspondingly ~45, 45, 21, 46, 38, and 28 respective arylene units (where each binaphthalene component is counted as a single arylene unit). CoMoCat SWNTs were obtained from Sigma-Aldrich as a freeze-dried powder and used as starting material for density gradient (DG) purification to obtain samples enriched with (6,5) chirality tubes. Raw SWNTs prepared via pulsed laser vaporization (PLV SWNTs) were obtained from NREL (Denver, Colorado); raw few-walled carbon nanotubes (FWNTs) prepared via chemical vapor deposition were obtained from Prof. J. Liu's Laboratory (Duke University, Durham, North Carolina); these materials were used without further purification.

Instrumentation. Electronic absorption spectra were recorded on a Varian 5000 UV−vis−NIR spectrophotometry system. CD spectra of the polymer−CNT samples were recorded on an Aviv Model 202 UV−vis CD spectrophotometer that uses a PMT detector and a Xe lamp light source (bandwidth 1 nm). All spectra were acquired via a single scan over the 200−700 nm range with 3 s exposure at each 2 nm step.

Computational Methods. CD spectra of the binaphthalene-based chiral polymers were simulated using the model compound *R*/*S*-1,1′-bi-2-naphthol and related derivatives (Figure 5C,D; Figure 9D,E) as a function of the torsional angle (ϕ = 50−120°) between the two naphthalene units along their respective chirality axes using time-dependent density functional theory (TDDFT//B3LYP/6-311+G**; Gaussian-09 software package[22]). First, structures of the model compounds were optimized for a fixed naphthalene−naphthalene torsional angle, keeping the two consecutive torsional angles (C9−C1−C1′−C9′ and C2−C1−C1′−C2′; see Figures 5C, 9D) constant using B3LYP/6-31+G basis functions. Rotatory strengths (length representation) were obtained via TDDFT calculations of 15−25 excited states for these DFT-optimized structures using the B3LYP/6-311+G** basis set. The CD spectra were then simulated by convoluting the individual Gaussian curves[23] using the GaussSum 2.2 program;[24] this approach utilizes the expression $\Delta\varepsilon(E) = \{2\Delta E/(2.296 \times 10^{-39}\, \pi^{1/2}\omega)\} \times R \exp[-\{2(E - \Delta E)/\omega\}^2]$,[23d] where $\Delta\varepsilon(E)$ is molar circular dichroism, R is rotatory strength, ω is bandwidth at 1/e peak height (= 0.3 eV), and ΔE is the TDDFT calculated transition energy. Note that the simulated spectra of Figures 5C and 9D are presented reversed in sign, to match the experimental spectra (which display an opposite Cotton effect due to their 6,6′ connectivity).

Molecular dynamics simulations were performed using the NAMD program.[25] Force field parameters were adapted from CHARMM potentials, developed using quantum mechanical calculations, and adapted from parameters reported in previous work.[20a,26] Computational details regarding the potential energy parameters and partial atomic charges are provided in the Supporting Information.

Structural Characterization. Transmission electron microscopy (TEM) images (JEOL TEM-2010; accelerate voltage, 200 kV) were obtained from samples prepared via drop casting on lacy Formvar copper grids stabilized with carbon followed by drying in a desiccator overnight. Atomic force microscopy (AFM; Digital Instruments Dimension 3100) images were obtained via intermittent contact mode (scan rate = 0.6 Hz, ambient temperature) using supersharp Si-tips (tip radius <5 nm, cantilever resonant frequency ~70 kHz). AFM samples were prepared by drop-casting SWNT suspensions on Si wafer surfaces (cleaned with acetone and 2-propanol); such samples were then desiccator-dried overnight. AFM data are presented with a first order plane fit.

Sample Preparation. Detailed sample preparation procedures are given in the Supporting Information. Sodium cholate (SC) dispersions of raw, as received carbon nanotube samples (SC-CNTs), e.g., SC-CoMoCat, SC-PLV, and SC-FWNT samples, were prepared using the standard ultrasonication centrifugation technique.[15d,20a] A 20-mL aqueous solution of SC (1 wt %) was sonicated with 8 mg of the corresponding CNT sample in direct contact with a tip horn sonicator (20 kHz; 12 W total power; at 0 °C), and centrifuged (90,000*g*; 0.5 h, 2×). The upper 60% of the suspension volume was collected and used as the starting material to prepare polymer-CNT samples. Surfactant solubilized (6,5) chirality enriched tube suspensions **SC-[(6,5) SWNTs]** were prepared in H_2O and D_2O solvents from an aqueous SC-CoMoCat dispersion using an established method.[21a] A **SC-[(6,5) SWNT]** sample in D_2O was used as a benchmark sample in various spectroscopic experiments.

General Procedure for the Preparation of Chiral Polymer-Wrapped Carbon Nanotube (poly-CNT) Suspensions. In brief, a 10-mL aqueous suspension of **SC-CNTs** (e.g., **SC-[(6,5) SWNTs]**, **SC-PLVs**, or **SC-FWNTs**) having a CNT concentration of ~0.1 mg/mL, was added slowly (over 3 h) to a 5-mL polymer solution (1.6 mg/mL).[21a] The mixture was stirred overnight and exchanged into a 5 mM carbonate/15 mM NaCl buffer (pH ~9) either using a Microcon centrifugal filter (YM-100; Millipore, Bedford, MA) or by filtering and washing through a 200 nm PTFE membrane (Millipore) with the appropriate buffer solution. Free, unbound polymer in each poly-CNT sample was removed via GPC: a 2 mL poly-CNT solution (CNT concentration of ~0.5 mg/mL) was injected into a series of two preparative columns (160 mm × 16 mm each; sephacryl-based separatory media) connected in the order of (a) S-500 [Sigma-Aldrich; MW fractionation range 40−20000 kDa (dextran)] and (b) S-200 [Sigma-Aldrich; MW fractionation range 1−80 kDa (dextran)], mounted on a GE/ÄKTApurifier HPLC system (GE Healthcare Bio-Science AB, Björkgatan, Uppsala, Sweden); samples were eluted with 5 mM carbonate/15 mM NaCl buffer (pH ~9) at a flow rate of 1 mL/min. Three-wavelength detection was utilized for all samples (carbon nanotubes were detected at 580 nm; phenylene-based polymers were detected at 315 and 440 nm, and porphyrin-based polymers were detected at 400 and 700 nm) in order to identify fractions that did not contain CNTs. For ***S*/*R*-PBN-Ph$_3$-**, ***S*-PBN(b)-Ph$_5$-**, and ***S*-PBN(b)-Ph$_4$PhCN**-wrapped CNT samples, a 5 mM carbonate/15 mM NaCl buffer in 3:7 MeOH/H_2O solvent mixture was used, while a 5 mM carbonate/15 mM NaCl buffer in 2:4:5 THF/MeOH/H_2O solvent mixture was used for ***R*-PBN-PZn$_2$-** and ***S*-PBN(b)-Ph$_2$PZn$_2$-**wrapped CNT samples. The fractions were collected as 1-mL aliquots; the poly-CNT fractions eluted first (~20−27 min), followed by the free, unbound polymers (~28−48 min; see Supplementary Figures S10 and S11). Fractions consisting of poly-CNTs (eluted at 20−27 min) were collected together and exchanged into D_2O via filtering, washing, and resuspension to provide final sample concentrations of ~1 mg/mL. The pH of these samples was adjusted to ~8 by adding an appropriate amount of 0.1 mM NaOD in D_2O, and the samples were stored in clean, sealed vials. Samples utilized for spectroscopic studies were diluted with the appropriate solvent to provide a CNT concentration of ~0.06 mg/mL.

RESULTS AND DISCUSSION

Theoretical calculations,[16a] including detailed molecular dynamics simulations,[27] have predicted that SWNTs induce a spontaneous conformation change in single-stranded DNAs (ssDNAs) that interact with the nanotube surface, resulting in self-assembled, wrapped polynucleotide-nanotube structures that take advantage of $\pi-\pi$ interactions between the faces of ssDNA bases and the SWNT. Considering only the attractive $\pi-\pi$ stacking interaction, purines experience higher binding energy than do the pyrimidines, with homopolymeric ssDNAs following a trend in binding energies where dG > dA > dT > dC.[27] Furthermore, MD simulations indicate that short ssDNAs can spontaneously bind to the SWNT surface in various configurations to generate both right- and left-handed helices, as well as loops and disordered structures within the range of accessible backbone conformations;[16a,27] highly varied right- and left-handed helical wrapping motifs are thus observed for ssDNA-SWNT superstructures that differ with respect to backbone torsional angles and the orientation of the adsorbed nucleobases, irrespective of SWNT chirality.[27] A decrease in

electrostatic repulsive interactions between the adjacent phosphate ions along the ssDNA backbone has been revealed as a key driver of helical wrapping.[27] Experimental data that probed the ssDNA dissociation kinetics indicate that the bound DNA strands in DNA-SWNT samples exist in equilibrium with unbound DNA strands and highlight that the stability of these ssDNA-SWNT superstructures are nucleobase-,[28] time-,[16b,28] and temperature-dependent.[28] For example, the homopolymeric $d(T)_{12}$-SWNT hybrid was found to have a $T_{1/2}$ (the temperature at which after 10 min incubation only 1/2 of the initial DNA-SWNT hybrids remain dispersed) of 71 °C, with respective dissociation rate and an equilibrium constants of 1.03 min^{-1} and 11.2 μM, congruent with the fact that large excesses ssDNA in solution are required to stabilize ssDNA-SWNT suspensions.

In this study, we synthesized a series of chiral binaphthalene (BN)-based semiconducting polymers: ***R*-PBN-Ph$_3$**, ***S*-PBN-Ph$_3$**, ***R*-PBN-PZn$_2$**, ***S*-PBN(b)-Ph$_5$**, ***S*-PBN(b)-Ph$_4$PhCN**, and ***S*-PBN(b)-Ph$_2$PZn$_2$** (Chart 1). For these aryleneethynylene polymers, palladium-catalyzed Sonogashira polycondensation reactions[29] were utilized to introduce a chiral 1,1′-bi-2-naphthol moiety at regular intervals along the polymer backbone; 6,6′-BN connectivity was exploited throughout these compositions. Synthetic conditions were modulated in order to produce polymers within the 15−22 kDa range, corresponding to polymeric strands composed of 21−46 total aromatic moieties; these length dimensions are comparable to that previously reported for the PNES polymer synthesized via Suzuki−Miyaura polycondensation reactions in neat water[20b] (see Supporting Information) and utilized to produce **PNES-SWNTs**.

Chiral polymer-wrapped SWNT suspensions were prepared readily by slowly mixing an aqueous solution of the desired polymer with presuspended, surfactant-coated carbon nanotube suspensions (SC-CNTs) following a previously established method.[21a,30] Favorable $\pi-\pi$ interactions between the polymer strands and the CNT surface drive the surfactant (SC) replacement process, resulting in polymer-wrapped CNT constructs.[20b,21a] Unbound polymers were removed via GPC (see Experimental Section; Supporting Information). To interrogate the stability of these polymer-wrapped CNT samples after removing unbound polymers from the suspension via GPC, these poly-CNTs were subjected to a second GPC separation; such GPC experiments, highlighted in Supplementary Figure S10B, reveal that no detectable polymer dewrapping occurs from these poly-CNT constructs over a time period of 10−14 days. The SWNT mass suspended in these chiral poly-CNT suspensions was estimated from the optical density of the E_{11} transition for [(6,5) SWNT] samples over the 980−1020 nm wavelength range, referenced to established literature benchmarks, where an optical density of 1 in a 1 cm quartz cell for a DNA-suspended [(6,5) SWNT] sample was taken to be ∼10 μg/mL.[16a,21a,31] The maximum (6,5) SWNT mass dispersion realized in aqueous solvent by these chiral polymers is ∼1−2 mg/mL; note that the steady-state vis−NIR absorption spectra highlighted in Figure 1 correspond to polymer-wrapped [(6,5) SWNT] samples in which the nanotube concentration is ∼0.05 mg/mL. The sharp E_{11} (980−1000 nm), E_{22} (∼570−580 nm), and E_{33} (∼348 nm) transitions for these polymer-wrapped [(6,5) SWNT] samples are similar to those observed for the SC-[(6,5) SWNT] reference spectrum (Figure 1), suggesting that these chiral polymers drive fully exfoliated SWNT suspensions consisting

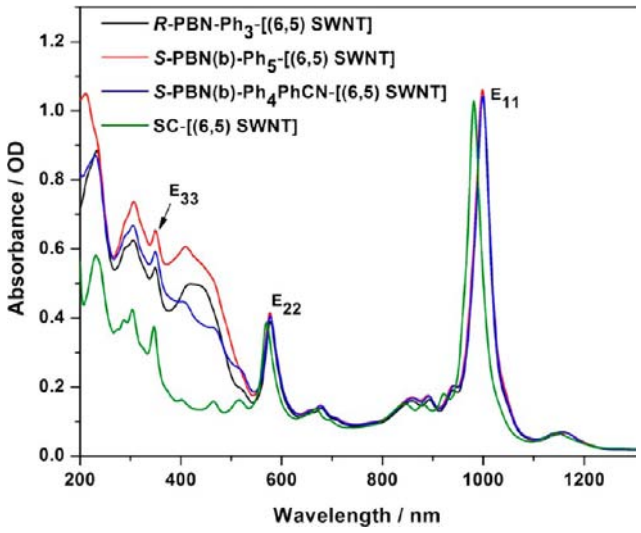

Figure 1. UV−vis−NIR absorption spectra of polymer-wrapped [(6,5) SWNT] samples. Poly-[(6,5) SWNT] suspensions of ***R*-PBN-Ph$_3$** (black), ***S*-PBN(b)-Ph$_5$** (red), and ***S*-PBN(b)-Ph$_4$PhCN** (blue) in 3:7 MeOH/D_2O solvent; the green spectrum corresponds to that for the aqueous SC-SWNT benchmark. Optical path length = 2 mm.; see Supplementary Figure S6 for corresponding electronic absorption spectra of the free polymers.

exclusively of individualized tubes (*vide infra*). As observed for **PNES-SWNTs**,[20b,21a,c] the prominent E_{11}, E_{22}, and E_{33} absorptions for these binaphthalene-based polymer-wrapped [(6,5) SWNT] samples exhibit respective spectral red shifts of 174−184 cm^{-1}, 213−243 cm^{-1}, and 165 cm^{-1} relative to the **SC-[(6,5) SWNT]** benchmark spectrum, consistent with significant $\pi-\pi$ interactions between each of these conjugated polymer backbones and the carbon nanotube.

High-resolution transmission electron microscopy (TEM) that interrogates ***R*-PBN-Ph$_3$-[PLV SWNT]** (Figure 2; Supplementary Figures S16 and S17) and ***S*-PBN-Ph$_3$-[PLV SWNT]** (Figure 3; Supplementary Figure S18) structures formed in aqueous solvent reveal that these samples are composed overwhelmingly of individualized nanotubes (>95%) that are periodically wrapped by single strands of these highly charged aryleneethynylene polymers. As observed for **PPES-SWNT**[20a] and **PNES-SWNT**[20b] compositions formed in aqueous media, these ***R*-PBN-Ph$_3$-SWNT** and ***S*-PBN-Ph$_3$-SWNT** assemblies manifest helically wrapped structures that feature small, repeating protuberances at regular nanometer-scale intervals along the SWNT axis that correspond to the polymer helical pitch length; note that this observed (8 ± 2 nm) helical pitch length evident for SWNTs wrapped by ***R*-PBN-Ph$_3$** and ***S*-PBN-Ph$_3$** is diminished compared to that observed previously for **PPES-SWNT** (13 ± 2 nm) and **PNES-SWNT** assemblies (10 ± 2 nm).[20] This marked repeating structural signature for helical wrapping by chiral ***R*-PBN-Ph$_3$** and ***S*-PBN-Ph$_3$** is also evidenced for two-tube bundles (Figure 2D; Supplementary Figure S18), where the observed helical pitch is shorter (7 ± 2 nm) than that of individualized tubes, indicating that helical pitch length tracks systematically with bundle cross section.

Considering the spatial orientation of the two naphthalene subunits of the chiral binaphthalenes, *R*-1,1′-bi-2-naphthol derived ***R*-PBN-Ph$_3$** strands are expected to form exclusively right-handed helical structures on SWNT surfaces, whereas corresponding *S*-1,1′-bi-2-naphthol-based ***S*-PBN-Ph$_3$** strands

dx.doi.org/10.1021/ja408430v | J. Am. Chem. Soc. 2013, 135, 16220−16234

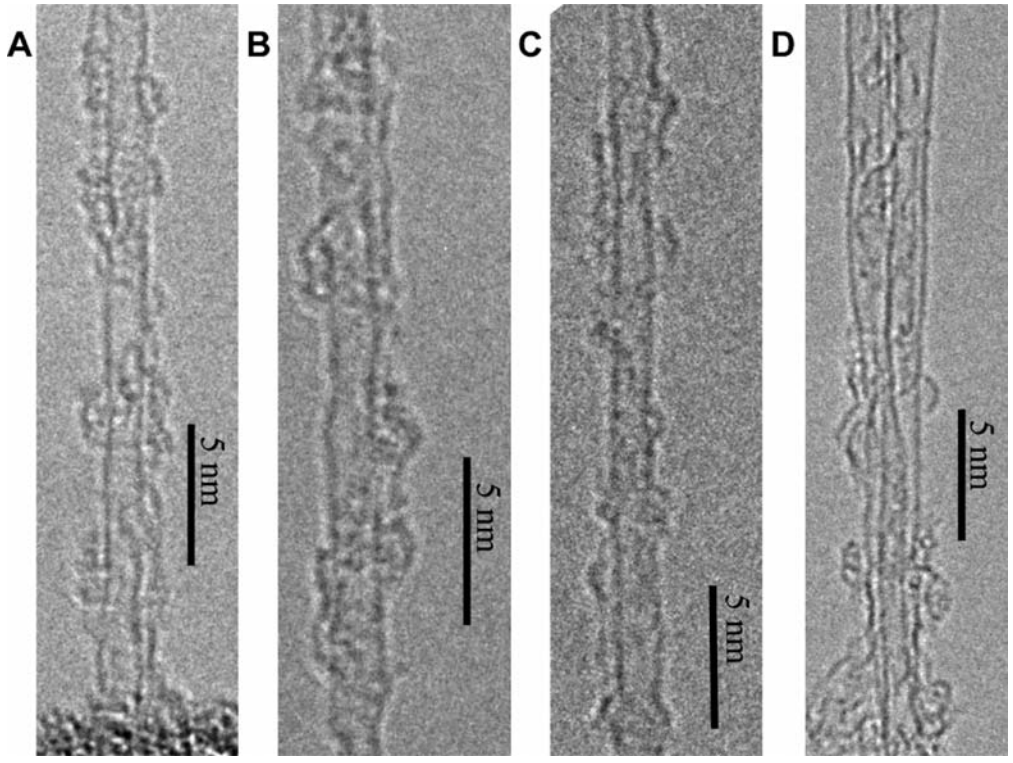

Figure 2. TEM images of ***R*-PBN-Ph$_3$**-wrapped [PLV SWNTs] obtained from aqueous suspension: (A–C) individualized tubes and (D) a two-tube bundle that highlight the expected right-handed helical wrapping structures. (See the Experimental Section for sample preparation conditions).

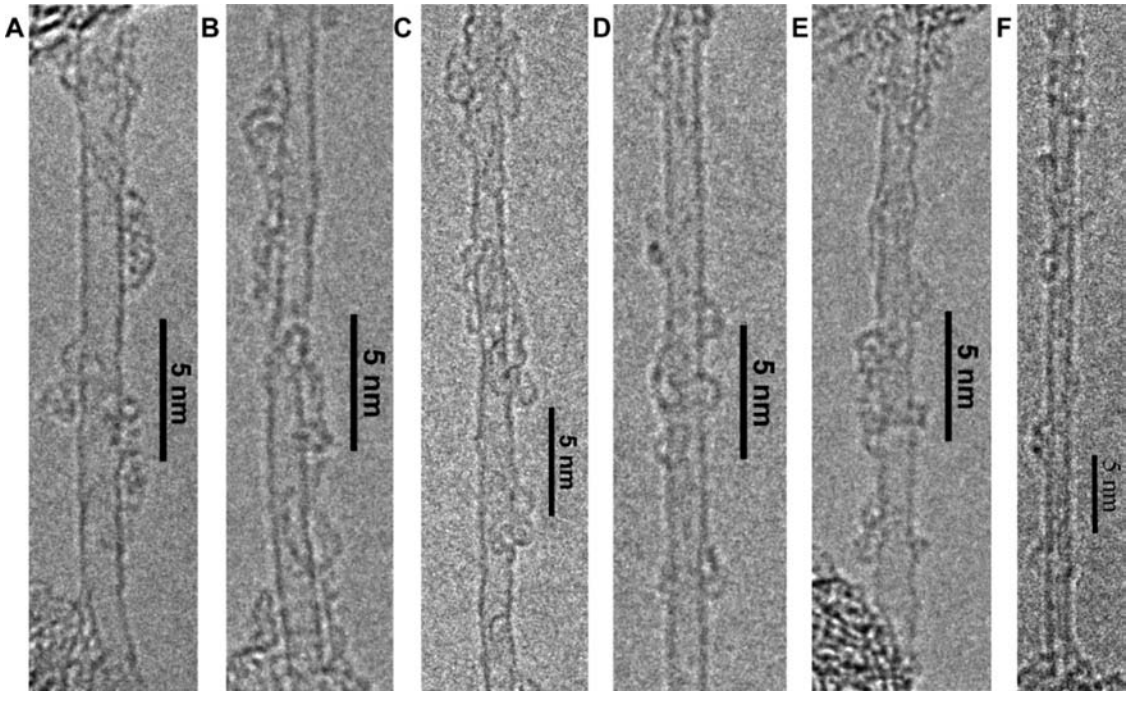

Figure 3. TEM images of ***S*-PBN-Ph$_3$**-wrapped [PLV SWNTs] obtained from aqueous suspension highlighting individualized tubes wrapped with expected left-handed (A–D) and unexpected right-handed (D, E) helical wrapping structures.

should generate analogous left-handed helical polymer-SWNT superstructures (Scheme 1). While HRTEM images of ***R*-PBN-Ph$_3$**- and ***S*-PBN-Ph$_3$**-wrapped SWNTs reveal significant preferences for the anticipated helical wrapping handedness, statistical analysis of these images indicate that at least 17% of the helical structures are formed with the "unexpected" handedness, that is, left-handed helical structures for ***R*-PBN-Ph$_3$**-wrapped SWNTs (Supplementary Figure S16D) and right-handed helical structures for ***S*-BN-Ph$_3$**-wrapped SWNTs (Figure 3E,F). The HRTEM images presented in Figure 3 also highlight that both the expected left- and unexpected right-handed helical structures formed by wrapping of ***S*-BN-Ph$_3$**

dx.doi.org/10.1021/ja408430v | *J. Am. Chem. Soc.* 2013, 135, 16220–16234

Scheme 1. Conformations of 1,1′-Bi-2-naphthol-Derived Polymer Chain Components and Their Possible Binding Modes at SWNT Surfaces[a]

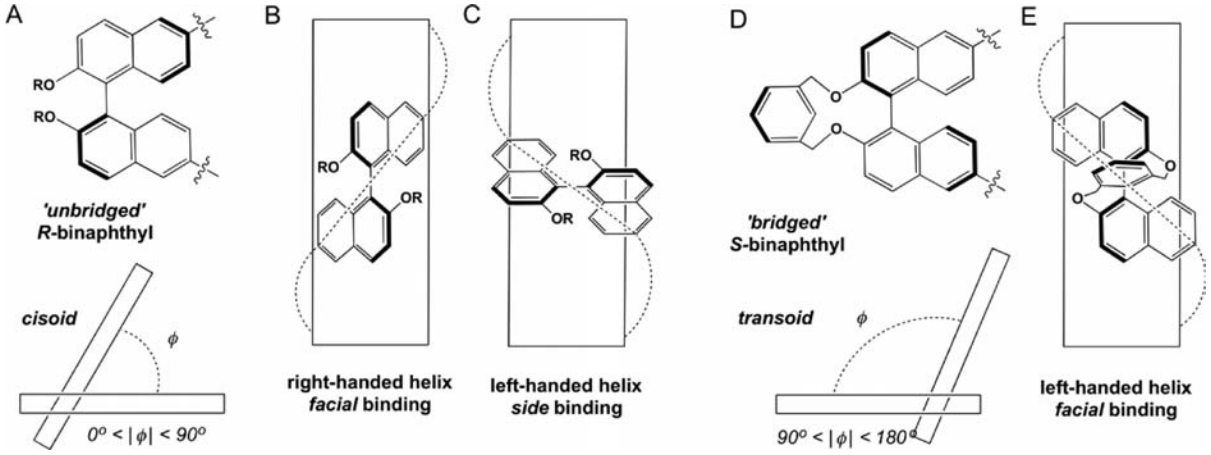

[a](A) The *cisoid* conformation adopted by the *unbridged R*-chirality binaphthyl unit. (B) Cartoon depicting "*cisoid-facial*" binding of an *R*-chirality binaphthalene to the SWNT surface in a right-handed helical superstructure. (C) Cartoon depicting the "*cisoid-side*" binding of an *R*-chirality binaphthalene to the SWNT surface in context of the "unexpected" left-handed helical superstructure. (D) The *transoid* conformation adopted by a *S*-chirality 2,2′-(1,3-benzyloxy)-*bridged*-1,1′-bi-2-naphthyl unit. (E) "*Transoid-facial*" binding mode of the *S*-chirality 2,2′-(1,3-benzyloxy)-*bridged*-1,1′-bi-2-naphthyl moiety with the SWNT surface in the context of a left-handed helical superstructure.

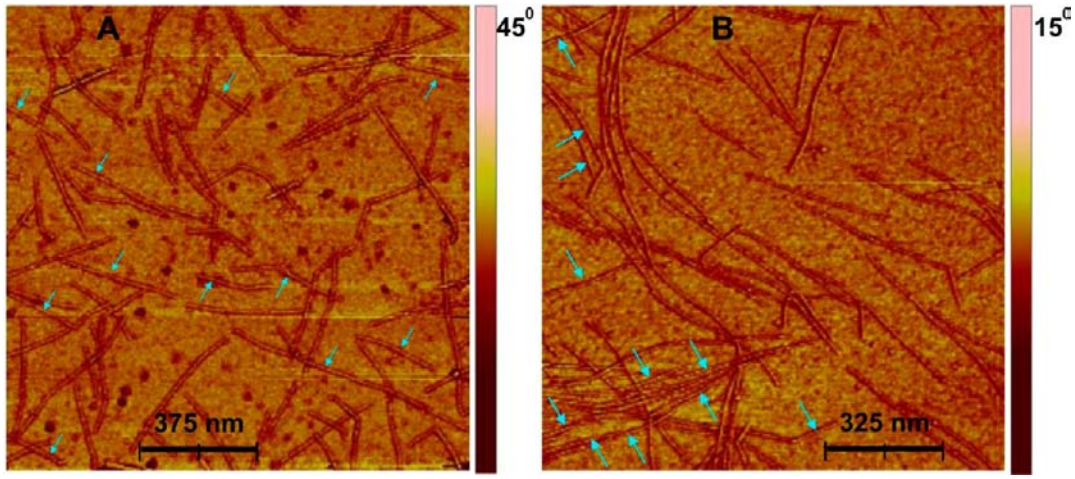

Figure 4. Phase images derived from intermittent contact mode AFM experiments of (A) ***R*-PBN-Ph$_3$-[PLV SWNTs]** and (B) ***S*-PBN-Ph$_3$-[PLV SWNTs]** from aqueous suspension on Si surfaces. Polymer-wrapped SWNT structures that evince the unexpected polymer helical wrapping chirality are marked with cyan arrows.

strands on the SWNT surface manifest comparable helical pitch lengths. Likewise, AFM images of ***R*-PBN-Ph$_3$-** and ***S*-PBN-Ph$_3$-**wrapped SWNTs dispersed in aqueous solvent (Figure 4A,B) corroborate the helical wrapping characteristics observed in the TEM images. Consistent with data previously reported for linear ionic aryleneethynylene PPES- and PNES-wrapped SWNT structures,[20] AFM experiments support the periodic helical wrapping of SWNTs by these chiral binaphthalene-based polymers. Data summarized in Figure 4 and Supplementary Figures S19 and S20 reveal that ∼20% of the ∼400 individual polymer-wrapped SWNT structures that were imaged evince the unanticipated helical handedness, similar to the corresponding data acquired via HRTEM.

To assess whether SWNT graphene helicity stemming from (n,m) chirality impacts to a discernible degree the nature of polymer wrapping handedness, a [-(6,5)]-enriched SWNT sample (∼30% ee; Supplementary Figure S12) was wrapped with both ***R*-PBN-Ph$_3$** and ***S*-PBN-Ph$_3$** polymers. Electronic absorption spectroscopic data (Supplementary Figure S13A) clearly evince an identical polymer to [-(6,5) SWNTs] ratio, indicating that the mass dispersion efficiency for [-(6,5) SWNTs] of both ***R*-PBN-Ph$_3$** and ***S*-PBN-Ph$_3$** polymers is the same. Likewise, AFM data summarized in Supplementary Figure S14 show clearly that the ***R*-PBN-Ph$_3$** and ***S*-PBN-Ph$_3$** polymer left- and right-handed helical wrapping statistics for [-(6,5)] enriched SWNTs do not differ relative to that evinced for a standard racemic (6,5)-enriched SWNT sample. Hence, for these chiral polymers that tightly wrap SWNTs, intrinsic nanotube helical chirality has no influence upon the helical-wrapping handedness observed on the SWNT surface. These UV−vis−NIR spectroscopic and microscopic (TEM and AFM) characterization data suggest strongly that the range of the accessible tertiary structures of these chiral ***R*-PBN-Ph$_3$** and ***S*-PBN-Ph$_3$** polymers in the solution must be responsible for the observed nonexclusive nature of the SWNT helical wrapping handedness.

dx.doi.org/10.1021/ja408430v | *J. Am. Chem. Soc.* 2013, 135, 16220−16234

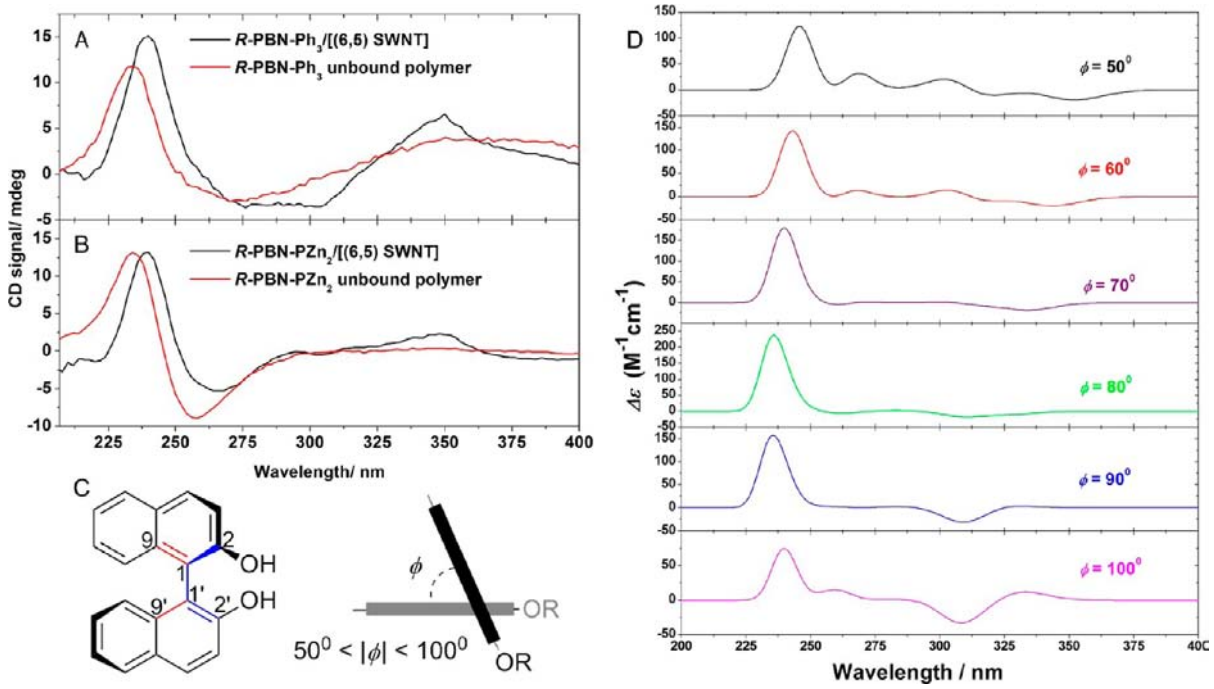

Figure 5. Comparative experimental CD spectra of *unbridged* binaphthalene polymers ***R*-PBN-Ph$_3$** and ***R*-PBN-PZn$_2$** benchmarked to computationally simulated spectra determined for the binaphthalene model compound (1,1′-bi-2-naphthol) as a function of naphthalene−naphthalene interplanar torsional angle along its chirality axis (C1−C1′). Experimental CD spectra recorded for (A) ***R*-PBN-Ph$_3$-[(6,5) SWNT]** (black), unbound ***R*-PBN-Ph$_3$** (red), and (B) ***R*-PBN-PZn$_2$-[(6,5) SWNT]** (black) and unbound ***R*-PBN-PZn$_2$** (red) samples in aqueous solvent. Optical path length = 1 cm; sample concentration = ∼0.008 mg SWNT/mL. (C) Structure of 1,1′-bi-2-naphthol. (D) 1,1′-Bi-2-naphthol CD spectral simulations at various torsional angles (ϕ) ranging from 50° to 100°. Note that two consecutive torsional angles (ϕ = C9−C1−C1′−C9′ and C2−C1−C1′−C2′), bonds marked in red and blue, respectively, were fixed at a given value during the structure optimization process (see Experimental Section).

To gain insight regarding the structural changes that these binaphthalene-based chiral polymers undergo upon SWNT binding, circular dichroism (CD) spectroscopic experiments were performed with ***R*-PBN-Ph$_3$**-dispersed SWNT samples and compared with analogous data obtained for the unbound ***R*-PBN-Ph$_3$** polymer in solution at an identical polymer concentration. Given the lack of literature precedent pertaining to CD spectroscopic characterization of related polymers, the CD spectrum of a model compound, 1,1′-bi-2-naphthol, was calculated using time-dependent density functional theory (TDDFT)-based computational methods (Figure 5); this structure was chosen because (i) the CD response of these binaphthalene-based chiral polymers will stem predominantly from this chiral moiety, and (ii) no circular dichroic response was observed for non-binaphthalene-containing aryleneethynylene polymers previously shown to wrap SWNTs (Supplementary Figure S15), for either their respective bound or unbound forms. To obtain a simulated CD spectrum over the 200−400 nm spectral window, 15 excited states were calculated via the TDDFT method for 1,1′-bi-2-naphthol structures for each of a number of selected naphthalene−naphthalene interplanar torsional angles (ϕ), in 10° increments.[23a−c] Figure 5 summarizes CD spectral data obtained for ***R*-PBN-Ph$_3$** and ***R*-PBN-PZn$_2$** in both nanotube-bound and unbound states (Figure 5A,B), the structural constraints used for 1,1′-bi-2-naphthol in the CD spectral calculations (Figure 5C), and the simulated spectra for 1,1′-bi-2-naphthol computed at various naphthalene−naphthalene interplanar torsional angles (Figure 5D). Comparative analysis of the experimental and simulated CD spectra, carried out as a function of binaphthalene torsional angle (ϕ), reveal that the unbound polymer (red spectrum in Figure 5A) manifests a CD spectrum virtually identical to that predicted for a binaphthalene unit that adopts a conformation having a naphthalene−naphthalene interplanar torsional angle of 65(±5)°; in this regard, note that a 2,2′-alkoxy substituted 1,1′-bi-2-naphthol has been determined computationally to adopt a similar torsional angle in $CHCl_3$ solution.[2b] The CD spectrum recorded for the ***R*-PBN-Ph$_3$**-wrapped SWNT sample (Figure 5A) reveals that the binaphthyl units of the polymer also adopt a similar conformation, exhibiting a CD spectral response consistent with a naphthalene−naphthalene interplanar torsional angle of 65(±5)°. Note that these comparative experimental and simulated CD spectroscopic results also rule out the possibility of a racemization process involving the 1,1′-binaphthalene unit as a possible origin for the ∼20% fraction of the unexpected helical chirality for the ***R*-PBN-Ph$_3$** and ***S*-PBN-Ph$_3$** polymer-wrapped SWNT assemblies observed in the AFM and TEM images (Figures 3 and 4); these findings are consistent with the substantial energetic barrier to binapthyl racemization (>20 kcal/mol).[32]

Scheme 1A depicts a binaphthalene unit in a *cisoid* conformation with a torsional angle $\phi \approx 60-70°$ between its two naphthalene subunits.[2b] On the basis of the data highlighted by the microscopic and spectroscopic experiments, we propose two distinct SWNT binding modes, *cisoid-facial* and *cisoid-side* (Scheme 1B and C, respectively) as likely interaction modes for these binaphthalene-based polymers with SWNTs that would account for both the observed expected and unexpected polymer helical wrapping chiralities at the nanotube surface. Though the *cisoid-facial* binding mode manifests a more

dx.doi.org/10.1021/ja408430v | J. Am. Chem. Soc. 2013, 135, 16220−16234

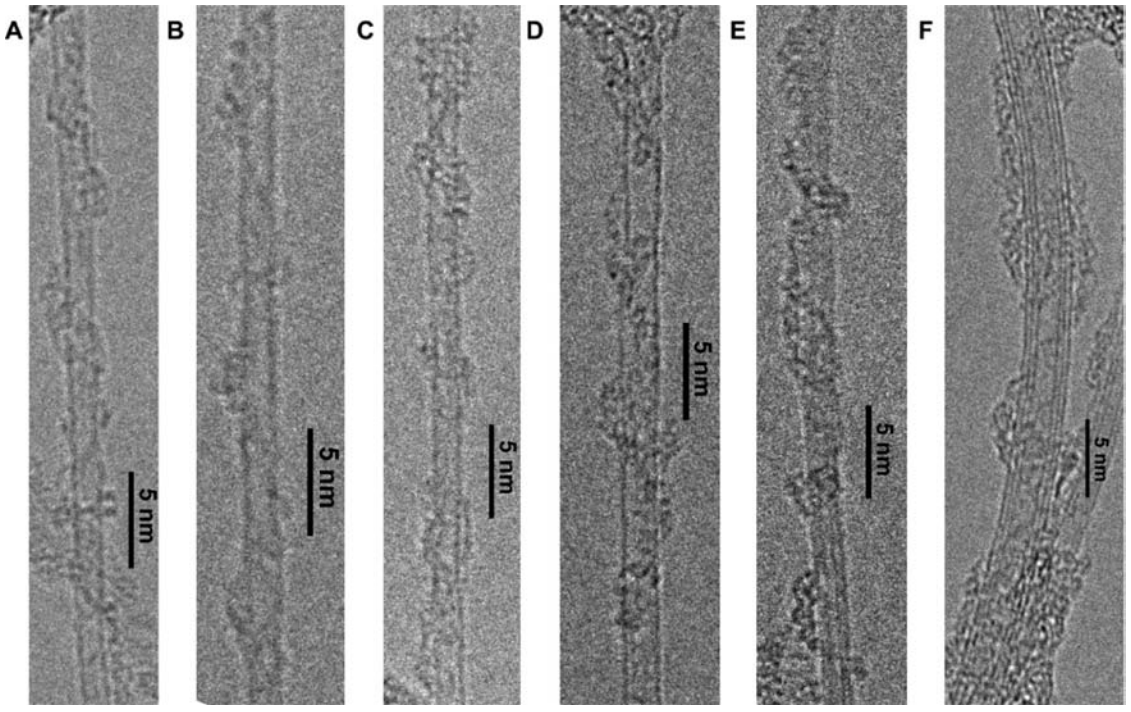

Figure 6. TEM images highlighting expected left-handed helical structures formed by ***S*-PBN(b)-Ph_5**-wrapped (A–D) [PLV SWNTs] (d = 1.4–2.4 nm) and (D, E) FWNTs (d = 2.8–3.5 nm) obtained from corresponding aqueous suspensions.

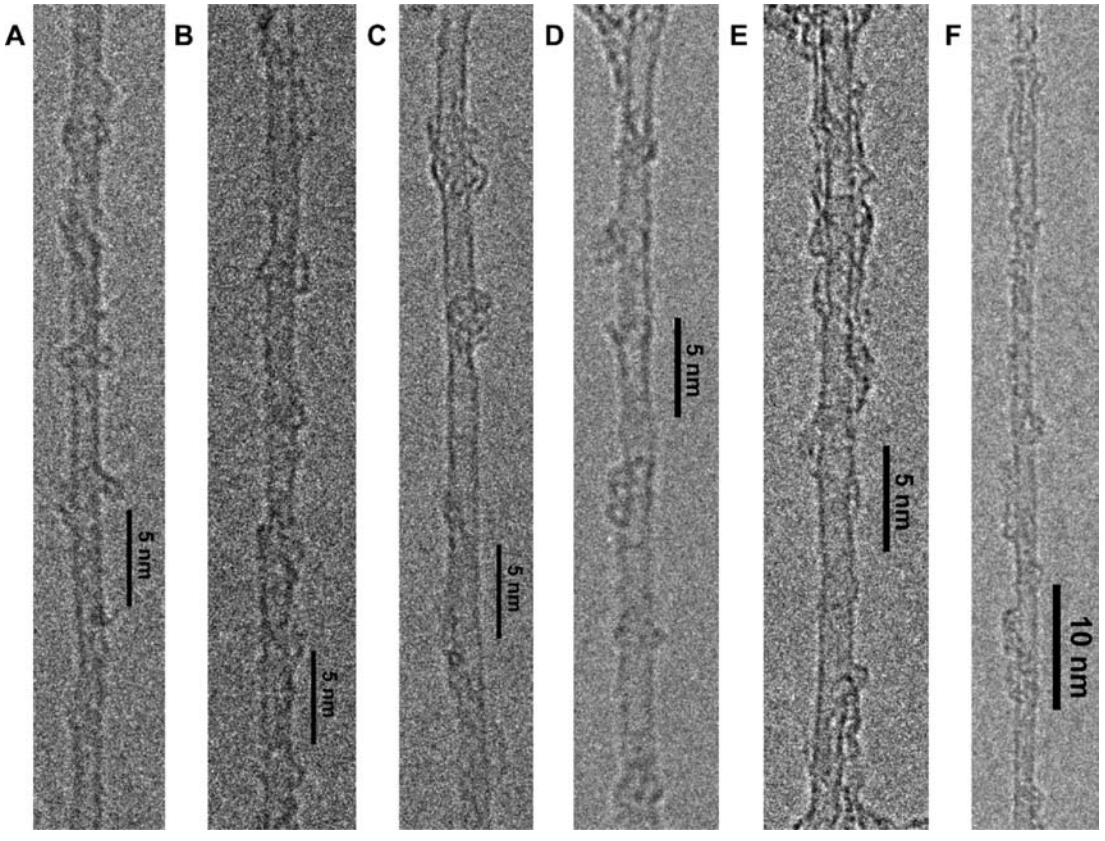

Figure 7. TEM images highlighting expected left-handed helical structures formed by ***S*-PBN(b)-Ph_4PhCN**-wrapped (A–C) and ***S*-PBN(b)-Ph_2PZn_2**-wrapped (D–F) [PLV SWNTs] (d = ∼1.4 nm) from corresponding aqueous suspensions.

extensive van der Waals interaction with the SWNT surface relative to that provided by the *cisoid-side* mode, we hypothesize that kinetic factors may play a critical role in the observed distribution of wrapping geometries. As the respective activation energies for dissociation of $d(C)_{12}$ and $d(T)_{12}$ are 24.4 and 14.8 kcal/mol,[28] and computational studies indicate

dx.doi.org/10.1021/ja408430v | *J. Am. Chem. Soc.* 2013, 135, 16220–16234

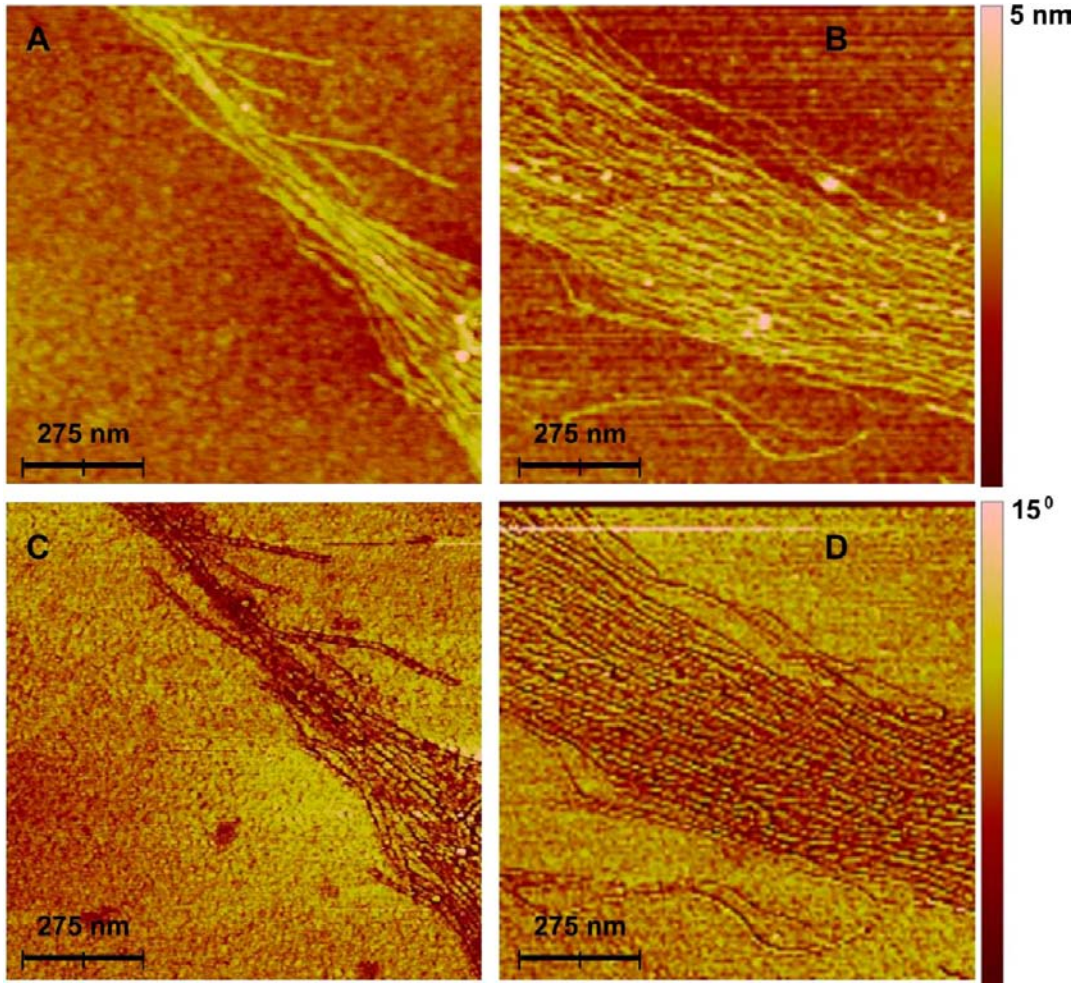

Figure 8. Topographic intermittent contact AFM images of (A, B) ***S*-PBN(b)-Ph$_4$PhCN-[(6,5) SWNTs]** from an aqueous suspension on a Si surface. (C, D) Corresponding phase images highlighting exclusive left-handed polymer wrapping along the SWNT surface. (See Experimental Section; Supplementary Figure S27)

that the binding energy for SWNTs helically wrapped by these ionic aryleneethynylene polymers is considerably higher (>54 kcal/mol),[20a] it is expected that in aqueous solvent, once a binaphthalene-containing polymeric strand binds to a SWNT surface in a *cisoid-facial* or *cisoid-side* geometry and subsequently wraps the SWNT surface, a change in binding-mode would be precluded by the high energetic barrier associated with dewrapping.

In light of these expected binding modes, we expect that increasing the naphthalene−naphthalene interplanar torsional angle of the 1,1′-binaphthalene moiety and restricting this geometry should provide more extensive van der Waals contact with the nanotube and promote *facial* binding of the SWNT by the polymer (Scheme 1D,E). Such exclusive *facial* binding should provide a means to control rigorously the helical handedness of these polymer-wrapped SWNT superstructures. To test this conjecture, we synthesized 2,2′-(1,3-benzyloxy)-*bridged* (b)-1,1′-bi-2-naphthol; this derivative features a naphthalene−naphthalene *bridging* 2,2′−1,3 benzyloxy tether that locks the torsional angle between the two naphthalene subunits along its C1−C1′ chirality axis. Polymers such as ***S*-PBN(b)-Ph$_5$**, ***S*-PBN(b)-Ph$_4$PhCN**, and ***S*-PBN(b)-Ph$_2$PZn$_2$** (Chart 1), based on this *bridged* binaphthalene derivative, were synthesized; note that for these polymers, two additional phenyleneethynylene units that bear the propoxysulfonate side chains were included in the backbone to provide appropriate aqueous solvent solubility (Chart 1). Helical SWNT superstructures derived from these *bridged* binaphthalene polymers were interrogated using both microscopic (AFM, TEM) and spectroscopic methods.

To understand how these *bridged* binaphthalene-based chiral polymers interact with the nanotube surface as a function of CNT metrical properties, CNTs of various diameters were utilized; these included DG-separated [(6,5) SWNTs] (d = 0.8 nm), [PLV SWNTs] ($d \approx$ 1.4 nm), and FWNTs (d = 2.8−3.5 nm). The HRTEM images highlighted in Figure 6 were obtained from ***S*-PBN(b)-Ph$_5$-[PLV SWNT]** (Figure 6A−D) and ***S*-PBN(b)-Ph$_5$-[FWNT]** (Figure 6E,F) samples; these images demonstrate clearly formation of the expected left-handed helical wrapping structures of the polymer on CNT surface. Likewise, HRTEM images summarized in Figure 7 for ***S*-PBN(b)-Ph$_4$PhCN-[PLV SWNT]** (Figure 7A−C) and ***S*-PBN(b)-Ph$_2$PZn$_2$-[PLV SWNT]** (Figure 7D−F) samples highlight similarly exclusive left-handed helical polymer-SWNT superstructures (see Supplementary Figures S21, S22, S23, and S24, respectively, for related TEM images of ***S*-PBN(b)-Ph$_5$-[PLV SWNTs]**, ***S*-PBN(b)-Ph$_5$-[FWNTs]**, ***S*-PBN(b)-Ph$_4$PhCN-[PLV SWNTs]**, and ***S*-PBN(b)-Ph$_2$PZn$_2$-[PLV SWNTs]**; Supplementary Figure S25 summarizes related data for ***S*-PBN(b)-Ph$_5$-**, ***S*-PBN(b)-Ph$_4$PhCN-**, and ***S*-PBN-**

dx.doi.org/10.1021/ja408430v | J. Am. Chem. Soc. 2013, 135, 16220−16234

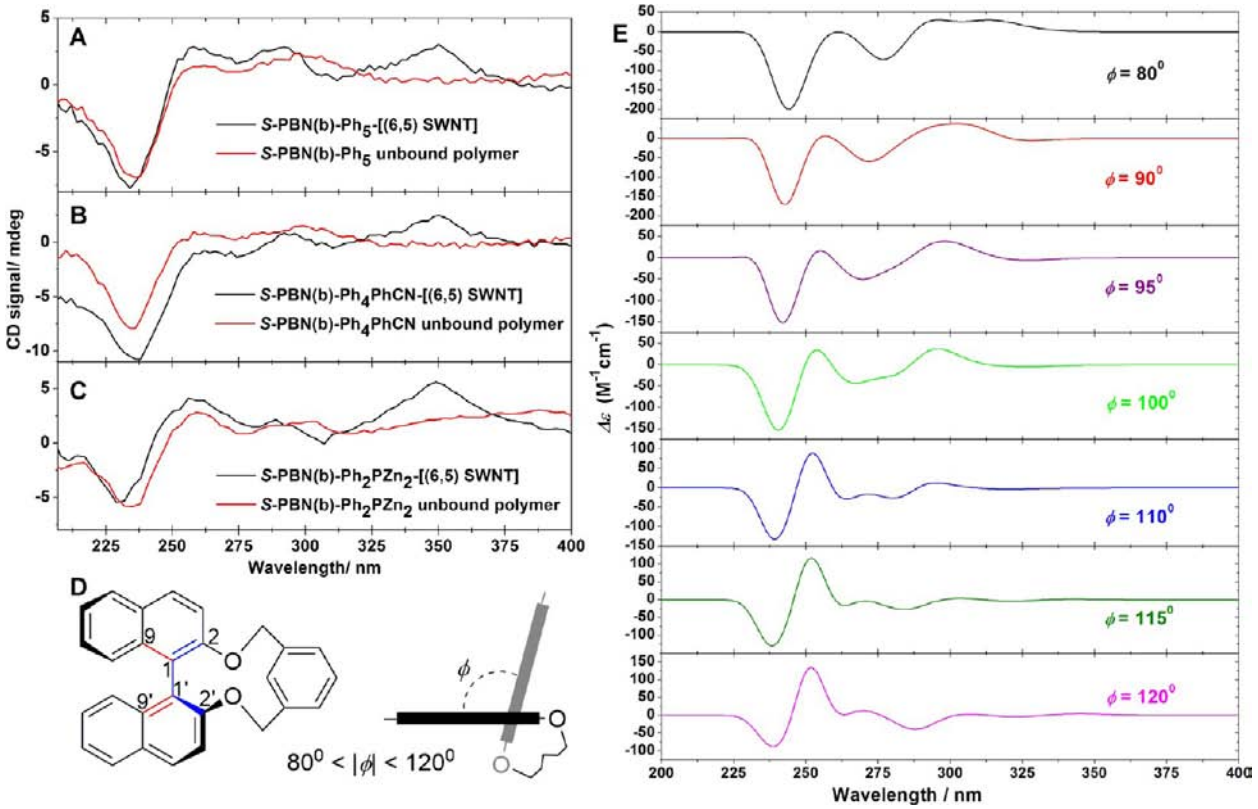

Figure 9. Comparative experimental CD spectra of polymers that incorporate the *bridged* binaphthalene unit, benchmarked to computationally derived spectra determined for the *bridged* binaphthalene model compound 2′-(1,3-benzyloxy)-*bridged*-1,1′-bi-2-naphthol as a function of naphthalene−naphthalene interplanar torsional angle along the C1−C1′chirality axis of the binaphthyl unit. Experimental CD spectral data recorded for: (A) ***S*-PBN(b)-Ph$_5$-[(6,5) SWNTs]**, (B) ***S*-PBN(b)-Ph$_4$PhCN-[(6,5) SWNTs]**, and (C) ***S*-PBN(b)-Ph$_2$PZn$_2$-[(6,5) SWNTs]**. Optical path length = 1 cm; sample concentration = 0.008 mg SWNT/mL. (D) Structure of the model compound used for the (E) TDDFT-based CD spectral simulations carried out as a function of the naphthalene−naphthalene interplanar torsional angle (ϕ). Note that two consecutive torsional angles (ϕ = C9−C1−C1′−C9′ and C2−C1−C1′−C2′), bonds marked in red and blue, respectively, were fixed at a given value during the structure optimization process (see Experimental Section; Figure 5).

(b)-Ph$_2$PZn$_2$-wrapped [(6,5) SWNTs]. A statistical analysis of ∼250 total TEM images reveals that these *bridged*-binaphthalene-based polymers form polymer-wrapped CNT constructs in which chiral polymer helical wrapping manifests an overwhelming preference (∼96%) for the expected left-handed helical superstructure (pitch-length = 8 ± 2 nm). Topographic intermittent contact AFM and corresponding phase images (Figure 8; Supplementary Figures S26 and S28) indicate that 97% of the ∼400 individual polymer-wrapped SWNT structures that were imaged evince the expected left-handed helical wrapping structure, similar to that discerned from the HRTEM data noted above. A height profile analysis (Supplementary Figures S26 and S27) shows that these exclusive left-handed helical superstructures based on [(6,5) SWNTs] evince a pitch-length of 9 ± 2 nm, similar to that determined in corresponding HRTEM experiments.

Analysis of the experimental CD spectroscopic data (Figure 9A−C) for ***S*-PBN(b)-Ph$_5$-[(6,5) SWNTs]**, ***S*-PBN(b)-Ph$_4$PhCN-[(6,5) SWNTs]**, and ***S*-PBN(b)-Ph$_2$PZn$_2$-[(6,5) SWNTs]** and their corresponding unbound polymer samples reveals that these polymers, in both the nanotube-bound and unbound states, adopt a structure in which the binaphthalene units exist in a *transoid* conformation consistent with a naphthalene−naphthalene interplanar torsional angle ϕ = 95−100°, as determined via TDDFT-based CD spectral simulations involving the binaphthalene model compound 2,2′-(1,3-benzyloxy)-*bridged*-1,1′-bi-2-naphthol (Figure 9D). These studies suggest that chiral polymers based on conformationally restricted *transoid* binaphthalene units can direct preferential *facial* binding of the polymer with the CNT and thereby dictate helically wrapped polymer-nanotube superstructures of predetermined chirality. This engineering insight, which assures a near-quantitative helical screw preference for semiconducting polymers that single-chain wrap SWNT surfaces, provides the means to (i) regulate the strength of interaction between an aryleneethynylene polymer and the SWNT surface, (ii) design robust conjugated polymer-SWNT superstructures in which optoelectronic and chirooptic properties can be extensively modulated, and (iii) develop new approaches to organize SWNTs in the solid state.[33]

To provide a comprehensive molecular perspective that spans length scales ranging from the local conformational restrictions of the bridged binaphthyl moiety to the global helical superstructures observed in the AFM and TEM data, molecular dynamics (MD) simulations were conducted for the chiral ***S*-PBN(b)-Ph$_5$** polymer wrapped around a SWNT in aqueous solvent. The model polymer comprised five repeat segments (n = 5, Chart 1) and an additional Ph$_5$ group, yielding a total of 35 aromatic subunits. Given that the adopted helical conformations and handedness of the polymer-wrapped SWNT superstructure are insensitive to the chirality of the underlying nanotube, an achiral (10,0) SWNT was selected for the

dx.doi.org/10.1021/ja408430v | J. Am. Chem. Soc. 2013, 135, 16220−16234

simulation, which has a diameter (7.8 Å) similar to that of the (6,5) SWNT (7.5 Å). Simulations were carried out with explicit water (TIP3P)[25,34] and counterions, yielding a total of 111,902 atoms. Since no desorption of the polymer was observed during the MD simulation process in our previous studies on related polyaryleneethyne-wrapped SWNT systems,[20a,35] the initial conformations of the polymer was chosen by aligning the ***S*-PBN(b)-Ph$_5$** polymer structure to a left-handed helical contour with pitch p = 8.0 nm and helical radius r = 0.736 nm, resulting in an initial polymer configuration that is in van der Waals contact with the nanotube carbon atoms. In this initial configuration, the internal naphthalene−naphthalene torsional angle ϕ of each binaphthyl unit was chosen as ϕ = 90°. The system was minimized and allowed to evolve; simulation details appear in the Supporting Information.

The simulation of the ***S*-PBN(b)-Ph$_5$-[(10,0) SWNT]** complex yielded a robust helical superstructure that maintained the expected left-handed helical handedness. Figure 10A depicts renderings of the ***S*-PBN(b)-Ph$_5$-[(10,0) SWNT]** complex at 20 ns intervals. The polymer preserves its initial left-handed helical configuration for the duration of the 80 ns trajectory.

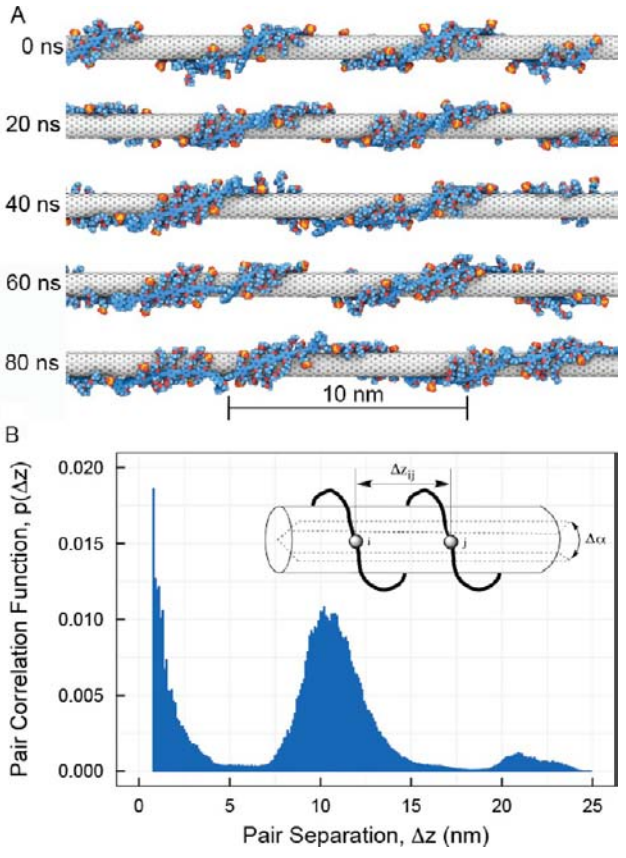

Figure 10. Helical superstructures of ***S*-PBN(b)-Ph$_5$** observed in molecular dynamics simulations. (A) Configurations sampled at 20 ns intervals (300 K), depicting the structures adopted by ***S*-PBN(b)-Ph$_5$**. The polymer was initially placed in a left-handed helix. (B) Pair correlation function $p(\Delta z)$ of backbone carbon atoms within ***S*-PBN(b)-Ph$_5$** (see eq 1), calculated using configurations sampled from the final 40 ns of the 80 ns simulation. (Inset) Depiction of the calculation of $p(\Delta z)$ within a cylindrical coordinate system: Δz_{ij} is the difference in z-coordinates of carbon atoms i and j when the separation in their polar angles (in the plane perpendicular to the nanotube axis) is less than $\Delta\alpha$ = 10°.

Since the polymer repeat unit contains multiple types of aromatic moieties, analyzing the trajectory via fits to ideal helical contours can be ambiguous; instead, the trajectory was analyzed through considering the pair correlation in the density of polymer backbone atoms within vertical "stripes" parallel to the tube along its surface; this quantity is in harmony with how helical pitch lengths are determined experimentally from TEM data. For an ideal helix, such a pair correlation function $p(\Delta z)$ will have as a function of the separation between atoms Δz a narrow peak at the origin (corresponding to atoms in the same or adjacent monomers), narrow peaks at multiples of the helical pitch, and minima with $p(\Delta z) \approx 0$ (corresponding to the groove of the ideal helix). The pairwise distribution function, $p(\Delta z)$, is evaluated using the following histogram function:

$$p(\Delta z) = \frac{\sum_{i<j} \delta(\Delta z,\ \Delta z_{ij},\ \delta z)\delta(\alpha_i,\ \alpha_j,\ \delta\alpha)}{\sum_{i<j} \delta(\alpha_i,\ \alpha_j,\ \delta\alpha)}$$

$$\text{where } \delta(x,\ y,\ \delta x) = \begin{cases} 1 \text{ for } |x - y| < \delta x \\ 0 \text{ otherwise} \end{cases} \quad (1)$$

where Δz_{ij} denotes the z-coordinate difference involving atoms i and j in the polymer, α_i denotes the radial angle coordinate of atom i in the x−y plane perpendicular to the nanotube axis (see Figure 10B), and δz and $\delta\alpha$ are the corresponding bin sizes for z and α, respectively. Here δz = 1 Å and $\delta\alpha$ =10°. An evaluation of the pair (density−density) correlation parallel to the nanotube axis for all backbone carbons in the polymer (35 subunits: aromatic phenyl, aromatic naphthyl, and ethyne carbons) shows characteristics expected for a helical configuration. Figure 10B shows this distribution for the ***S*-PBN(b)-Ph$_5$** polymer initially placed in a left-handed helix and is evaluated for the final 40 ns of the trajectory. The increasing amplitude for Δz < 3 nm corresponds to carbon atoms within the same and adjacent monomers. The distribution has near-zero amplitude over 4−8 nm and a large peak located at 10 nm, consistent with a persistent helical structure of pitch 10 nm. This value is consistent with the experimentally inferred helical pitch from the HRTEM (8 ± 2 nm) and AFM studies (9 ± 2 nm).

The simulation results reveal how the bridged binaphthyl units brace the left-handed helical structure while promoting contact of the arylene-ethynylene backbone with the SWNT. The torsional angle ϕ of the binaphthyl units within the ***S*-PBN(b)-Ph$_5$** polymer fluctuate about a well-defined average value, ϕ = 120(±8)° (Figure 11A,B). The binaphthyl moieties take on the transoid (ϕ > 90°) facial conformation (Scheme 1), consistent with the CD data. For this transoid conformation, the nanotube cross section is interior to ϕ of each binaphthyl unit, and viewed down the helical (nanotube) axis, the binaphthyl units envelop the circular nanotube. The naphthylene rings make extensive van der Waals contact with the carbon atoms of the SWNT (Figure 11B). The carbon atoms of adjacent phenylene-ethynylene units are also in van der Waals contact with the SWNT, as seen in studies of related aryleneethynylene polymers.[20,35] The distribution of ϕ for a simulation of the isolated ***S*-BN(b)** unit is centered about transoid conformations and has substantial overlap with that observed in the wrapped polymer (Figure 11C). Thus the ***S*-BN(b)** moiety is poised for formation of the left-handed helical superstructure. The unbridged ***S*-BN**, however, exhibits a much broader distribution $P(\phi)$ (Figure 11D) and populates both

dx.doi.org/10.1021/ja408430v | J. Am. Chem. Soc. 2013, 135, 16220−16234

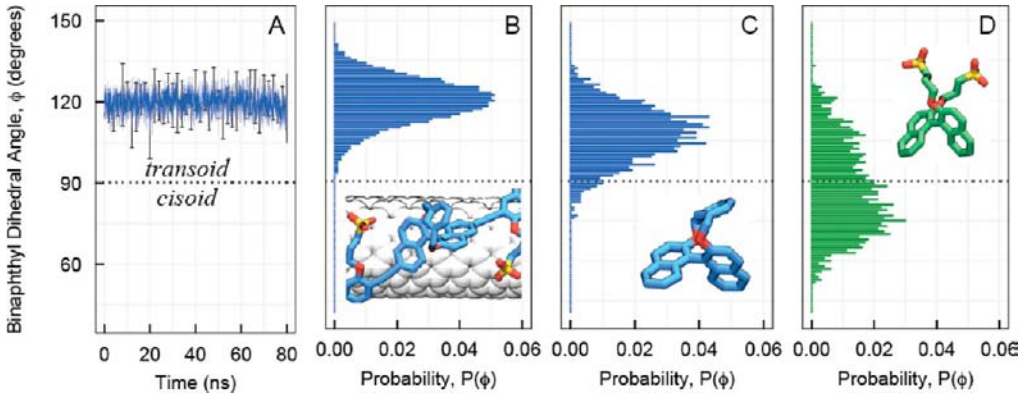

Figure 11. Binaphthyl dihedral angle ϕ data from simulations (see Scheme 1). (A) Time evolution of the average of ϕ for ***S*-PBN(b)-Ph$_5$**, which remained wrapped in a left-handed helix for the entire 80 ns simulation. At each time point (sampled configuration), the average and standard deviation of ϕ are calculated using the values observed for the bridged binaphthyl units of the polymer. Representative error bars are ±1 standard deviation and are only displayed for 1% of the sampled configurations. (B) Distribution $P(\phi)$ from the ***S*-PBN(b)-Ph$_5$-[(10,0) SWNT]** simulations. Configurations sampled every 20 ps over the interval 40−80 ns were used in the calculation of this histogram. A rendering of a subsegment where ϕ = 120° is shown. (C) Distribution $P(\phi)$ for an isolated bridged binaphthyl unit ***S*-BN(b)** (see Supplementary Figure S30) in aqueous solvent. Rendering of sampled conformation where ϕ = 107° is shown. (D) Distribution $P(\phi)$ for an isolated unbridged binaphthyl moiety ***S*-BN** in aqueous solvent. Rendering of sampled conformation where ϕ = 87° is shown. Distributions in panels C and D were calculated using configurations sampled every 20 ps over a 40 ns simulation at 300 K.

transoid and *cisoid* conformations (Scheme 1). This greater degree of conformational variability is consistent with the ability of the unbridged PBN polymers to exhibit no strong preference for left- and right-handed helical structures.

In order to exemplify how rigorous engineering of the helical screw preference for semiconducting polymers that single-chain wrap SWNT surfaces provides new opportunities for regulating the optoelectronic properties of semiconducting polymer-SWNT superstructures, chiral polymers that incorporate *meso*-to-*meso* ethyne-bridged bis[(porphinato)zinc][36] (PZn_2) units were synthesized (Chart 1). PZn_2 possesses (i) a low energy $\pi-\pi^*$ excited state polarized along its long molecular axis, (ii) cation and anion radical states that are globally delocalized, (iii) a large polarizability, (iv) intensely absorbing $S_0 \rightarrow S_n$ transition manifolds that overlap with the (6,5) SWNT E_{33} and E_{22} transitions, and (v) a low energy x-polarized $S_0 \rightarrow S_1$ absorption band that tails into the (6,5) SWNT E_{11} absorption. Further, because (i) PZn_2 features potentiometrically determined HOMO and LUMO levels[36f] close in energy to the respective valence and conduction bands of small-diameter SWNTs,[37] and (ii) related *meso*-to-*meso* butadiyne-bridged (porphinato)zinc oligomers have been shown by Anderson to interact strongly with nanotube surfaces,[38] added motivation was provided to produce PZn_2-based chiral semiconducting polymers that helically wrap SWNTs.

Vis−NIR absorption spectroscopic data summarized in Figure 12 reveal that the (6,5) SWNT E_{11} transition (~1017 nm) shows respective spectral red shifts of 350 and 380 cm^{-1} in ***R*-PBN-PZn$_2$-[(6,5) SWNT]** and ***S*-PBN(b)-Ph$_2$PZn$_2$-[(6,5) SWNT]** samples relative to the SC-[(6,5) SWNT] benchmark: SWNT E_{11} transition manifold shifts of this magnitude lack precedent in SWNT assemblies involving conjugated polymers. For these samples, any spectral perturbations of the SWNT E_{22} transition are masked due to the overlap of the PZn_2-based Q_y-derived transition manifold over the 570−580 nm region. Note that relative to the PZn_2 Q_x-derived transition manifold of the ***S*-PBN(b)-Ph$_2$PZn$_2$** polymer (λ_{max} ~735 nm; fwhm ~2750 cm^{-1}; Figure 12B), the analogous manifold of the ***S*-PBN(b)-Ph$_2$PZn$_2$-[(6,5) SWNT]** superstructure both extensively broadens (fwhm ~4050 cm^{-1}) and red shifts (940 cm^{-1}). Interestingly, an analogous comparison of the Q_x-derived transition manifolds for the ***R*-PBN-PZn$_2$** polymer and the ***R*-PBN-PZn$_2$-[(6,5) SWNT]** superstructure highlights a similar magnitude spectral red shift (~950 cm^{-1}) for the polymer-wrapped nanotube but shows no spectral absorption band shape evolution for the ***R*-PBN-PZn$_2$-[(6,5) SWNT]** construct: both ***R*-PBN-PZn$_2$** and ***R*-PBN-PZn$_2$-[(6,5) SWNT]** manifest similarly broad Q_x-derived transition manifolds (fwhm ~1800 cm^{-1}). These data indicate that the *bridged*, *transoid* binaphthalene-based PZn_2 polymer, ***S*-PBN(b)-Ph$_2$PZn$_2$**, manifests a stronger polymer-SWNT interaction relative to its *unbridged* ***R*-PBN-PZn$_2$** analogue. HRTEM (Supplementary Figure S25) and CD spectroscopic data (Figure 9C) obtained for ***S*-PBN(b)-Ph$_2$PZn$_2$-[(6,5) SWNTs]** are congruent with this picture: AFM data summarized in Supplementary Figure S29 show clearly that the left- and right-handed helical wrapping statistics for the *unbridged* ***R*-PBN-PZn$_2$-[(6,5) SWNT]** sample are similar to that evinced for ***R*-PBN-Ph$_3$-[(6,5) SWNTs]** (Supplementary Figure S14). Similarly, note that the CD spectroscopic data (Figure 5**B**) indicate that the conformation adopted by the *unbridged* binap units in ***R*-PBN-PZn$_2$-[(6,5) SWNTs]** corresponds to a *cisoid* naphthalene−naphthalene torsional angle of ~66°, as seen for the other *unbridged* binap polymers. While the precise origins of the more dramatic PZn_2-based spectral perturbations evident for ***S*-PBN(b)-Ph$_2$PZn$_2$-[(6,5) SWNTs]** relative to ***R*-PBN-PZn$_2$-[(6,5) SWNTs]** remain to be investigated, these data suggest that the combination of the uniform binaphthalene-SWNT facial interaction and exclusive left-handed helical wrapping made possible by the conformationally restricted *transoid* binaphthalene units of ***S*-PBN(b)-Ph$_2$PZn$_2$** (Scheme 1, Figure 9, Figure 12; Supplementary Figure S25) lead to enhanced electronic and excitonic interactions between the SWNT and the PZn_2 chromophoric unit of the ***S*-PBN(b)-Ph$_2$PZn$_2$** polymer.

dx.doi.org/10.1021/ja408430v | J. Am. Chem. Soc. 2013, 135, 16220−16234

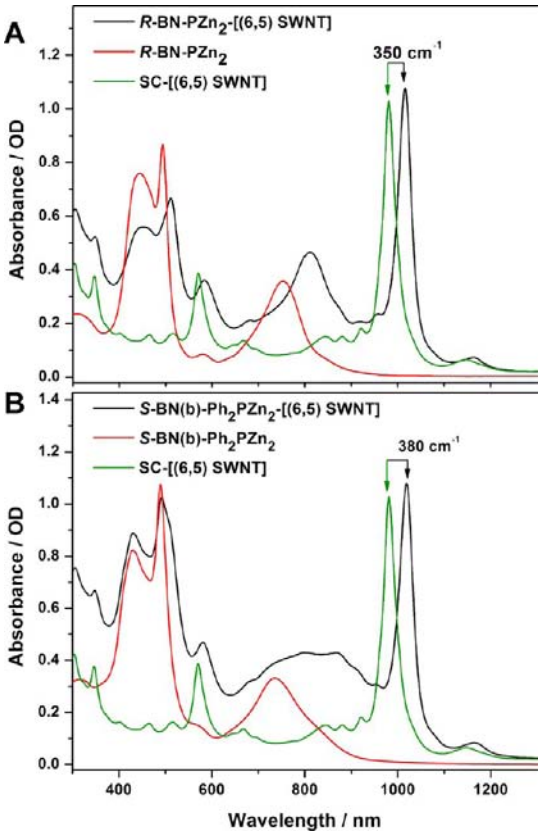

Figure 12. Electronic absorption spectra of (A) ***R*-PBN-PZn$_2$-[(6,5) SWNT]** (black) and the unbound ***R*-PBN-PZn$_2$** polymer (red) and (B) ***S*-PBN(b)-Ph$_2$PZn$_2$-[(6,5) SWNT]** (black) and the unbound ***S*-PBN(b)-Ph$_2$PZn$_2$** (red) polymer in 2:4:5 THF/MeOH/D_2O solvent. Unbound polymer samples were prepared to provide a polymer concentration in solution identical to that of their corresponding polymer-wrapped SWNT suspension. The electronic absorption spectrum of the SC-[(6,5) SWNT] benchmark (green) in D_2O solvent corresponds to that for a SWNT concentration identical to that of the polymer-wrapped [(6,5) SWNT] samples: the relative peak positions of the E_{11} and E_{22} transitions for [(6,5) SWNTs] are marked with arrows, highlighting the spectral red shifts that derive from polymer wrapping. Optical path length = 2 mm. (See Experimental Section; Supporting Information).

CONCLUSION

While chiral polymers, such as ssDNAs, have been established to helically wrap single-walled carbon nanotubes (SWNTs), the resulting ssDNA-SWNT hybrids manifest both right- and left-handed helical SWNT assemblies, indicating that intrinsic polymer helical chirality is in general insufficient to dictate the helical chirality of polymer-nanotube constructs. This work describes the first general method to control rigorously the handedness of the helically wrapped polymer-SWNT superstructures.

Chiral polymers, closely related to linear, conjugated, highly charged poly(aryleneethynylene)s that have been established previously to exfoliate, individualize, and disperse SWNTs in both water and organic solvents via a single chain helical wrapping mechanism,[20b] were synthesized. These polymers feature a chiral 1,1′-bi-2-naphthol moiety (BN) at regular intervals along their respective polymer backbones and vary widely in electronic structure (Chart 1). While polymers ***R*-PBN-Ph$_3$**, ***S*-PBN-Ph$_3$**, and ***R*-PBN-PZn$_2$** (Chart 1), which utilize either an (*R*)- or (*S*)-1,1′-bi-2-naphthol component in their respective conjugated backbones, manifest HRTEM and AFM images of wrapped SWNTs that reveal significant preferences for the anticipated helical wrapping handedness, rigorous statistical analyses of these images indicate that ∼20% of the helical structures are formed with the "unexpected" handedness (e.g., left-handed helical structures for ***R*-PBN-Ph$_3$**-wrapped SWNTs and right-handed helical structures for ***S*-BN-Ph$_3$**-wrapped SWNTs). CD spectroscopic data, coupled with TDDFT-based computational simulations that correlate the spectral signatures of semiconducting polymer-wrapped SWNT assemblies with the structural properties of the chiral 1,1′-binaphthalene unit suggest strongly that two distinct binaphthalene SWNT binding modes, *cisoid-facial* and *cisoid-side* (Scheme 1), are possible for these polymers, with the latter mode responsible for inversion of helical chirality and the population of polymer-SWNT superstructures that feature the unexpected polymer helical wrapping chirality at the nanotube surface.

Analogous polymers were synthesized that feature a 2,2′-(1,3-benzyloxy)-*bridged* (b)-1,1′-bi-2-naphthol unit (BN(b)): this 1,1′-bi-2-naphthol derivative is characterized by a *bridging* 2,2′−1,3 benzyloxy tether that locks the torsional angle between the two naphthalene subunits along its C1−C1′ chirality axis. Similar microscopic, spectroscopic, and computational studies determine that chiral polymers based on conformationally restricted *transoid* binaphthalene units (***S*-PBN(b)-Ph$_5$**, ***S*-PBN(b)-Ph$_4$PhCN**, and ***S*-PBN(b)-Ph$_2$PZn$_2$**; Chart 1) direct preferential *facial* binding of the polymer with the SWNT and thereby guarantee helically wrapped polymer-nanotube superstructures of fixed chirality. Molecular dynamics simulations of ***S*-PBN(b)-Ph$_5$** support this picture for specifying both the pitch and the chirality of such helical superstructures.

In order to underscore the extent to which these designs can be utilized to manipulate the electro-optic properties of semiconducting polymer-SWNT hybrids, chiral polymers ***R*-PBN-PZn$_2$** and ***S*-PBN(b)-Ph$_2$PZn$_2$** (Chart 1) were synthesized. These polymers feature a *meso*-to-*meso* ethyne-bridged bis[(porphinato)zinc] backbone (PZn_2) component, a chromophoric unit that possesses a large polarizability, intensely absorbing $S_0 \rightarrow S_n$ transition manifolds that overlap with the (6,5) SWNT E_{33} and E_{22} transitions, a low energy x-polarized $S_0 \rightarrow S_1$ absorption band that tails into the (6,5) SWNT E_{11} absorption,[13c,21a] and potentiometrically determined HOMO and LUMO levels[36f] close in energy to the respective valence and conduction bands of small-diameter SWNTs. The (6,5) SWNT E_{11} transition (∼1017 nm) shows respective spectral red shifts of 350 and 380 cm^{-1} for ***R*-PBN-PZn$_2$-[(6,5) SWNT]** and ***S*-PBN(b)-Ph$_2$PZn$_2$-[(6,5) SWNT]** samples relative to standard surfactant-dispersed (6,5) SWNT] benchmarks: such E_{11} transition manifold shifts lack precedent in noncovalent SWNT assemblies involving conjugated organic structures. These electronic absorption spectral data further indicate that the combination of the uniform binaphthalene-SWNT facial interaction and exclusive left-handed helical wrapping made possible by the conformationally restricted *transoid* binaphthalene units of ***S*-PBN(b)-Ph$_2$PZn$_2$** lead to enhanced electronic and excitonic interactions between the SWNT and the PZn_2 chromophoric unit in ***S*-PBN(b)-Ph$_2$PZn$_2$-[(6,5) SWNT]** constructs that are absent in corresponding ***R*-PBN-PZn$_2$-[(6,5) SWNT]** samples.

In summary, the design insights described herein enable enantioselective control of the helical screw axis of semi-

dx.doi.org/10.1021/ja408430v | J. Am. Chem. Soc. 2013, 135, 16220−16234

conducting polymers that single-chain wrap SWNT surfaces. We posit that this work opens up new opportunities to (i) regulate the strength of excitonic and electronic interactions between an aryleneethynylene polymer and the nanotube surface, (ii) engineer robust conjugated polymer-SWNT superstructures in which optoelectronic and chirooptic properties can be extensively modulated, and (iii) develop new approaches to organize SWNTs in the solid state.[33]

■ ASSOCIATED CONTENT

Supporting Information

Polymer synthesis and characterization, polymer-CNT sample preparation, additional spectroscopic, microscopic characterization data for chiral polymer-wrapped SWNTs, computational parameters and topologies, including partial charges for the simulated binaphthyl polymer. This material is available free of charge via the Internet at http://pubs.acs.org.

■ AUTHOR INFORMATION

Corresponding Authors

saven@sas.upenn.edu
michael.therien@duke.edu

Notes

The authors declare no competing financial interest.

■ ACKNOWLEDGMENTS

This work was funded by the Division of Chemical Sciences, Geosciences, and Biosciences, Office of Basic Energy Sciences, of the U.S. Department of Energy through Grant DE-SC0001517. Support was provided by the University of Pennsylvania's Nano/Bio Interface Center (NSF NSEC DMR 08-32802) and infrastructural support by the Laboratory for the Research on the Structure of Matter (NSF MRSEC DMR 11-20901). This research was supported in part by the National Science Foundation through XSEDE resources provided by NICS under grant number TG-CHE110041. C.D.V.B. and J.G.S. thank Christopher MacDermaid and Colleen Murrett for assistance with the modeling calculations.

■ REFERENCES

(1) Saenger, W. *Principles of Nucleic Acid Structure*; Springer-Verlag: New York, 1984.

(2) (a) Koeckelberghs, G.; Verbiest, T.; Vangheluwe, M.; Groof, L. D.; Asselberghs, I.; Picard, I.; Clays, K.; Persoons, A.; Samyn, C. *Chem. Mater.* **2005**, *17*, 118−121. (b) Mori, T.; Kyotani, M.; Akagi, K. *Macromolecules* **2008**, *41*, 607−613. (c) Yashima, E.; Maeda, K.; Furusho, Y. *Acc. Chem. Res.* **2008**, *41*, 1166−1180. (d) Maeda, K.; Wakasone, S.; Shimomura, K.; Ikai, T.; Kanoh, S. *Chem. Commun.* **2012**, *48*, 3342−3344.

(3) Ousaka, N.; Takeyama, Y.; Iida, H.; Yashima, E. *Nat. Chem.* **2011**, *3*, 856−861.

(4) Verbiest, T.; Sioncke, S.; Persoons, A.; Vyklický, L.; Katz, T. J. *Angew. Chem., Int. Ed.* **2002**, *41*, 3882−3884.

(5) Verbiest, T.; Elshocht, S. V.; Kauranen, M.; Hellemans, L.; Snauwaert, J.; Nuckolls, C.; Katz, T. J.; Persoons, A. *Science* **1998**, *282*, 913−915.

(6) Göhler, B.; Hamelbeck, V.; Markus, T. Z.; Kettner, M.; Hanne, G. F.; Vager, Z.; Naaman, R.; Zacharias, H. *Science* **2011**, *331*, 894−897.

(7) Lee, E.; Hammer, B.; Kim, J.-K.; Page, Z.; Emrick, T.; Hayward, R. C. *J. Am. Chem. Soc.* **2011**, *133*, 10390−10393.

(8) (a) Marini, D. M.; Hwang, W.; Lauffenburger, D. A.; Zhang, S.; Kamm, R. D. *Nano Lett.* **2002**, *2*, 295−299. (b) Yamamoto, T.; Fukushima, T.; Aida, T. In *Advanced in Polymer Science*; Springer: Berlin, 2008; Vol. *220*, 1−27; (c) Diegelmann, S. R.; Gorham, J. M.; Tovar, J. D. *J. Am. Chem. Soc.* **2008**, *130*, 13840−13841. (d) Peterca, M.; Percec, V.; Imam, M. R.; Leowanawat, P.; Morimitsu, K.; Heiney, P. A. *J. Am. Chem. Soc.* **2008**, *130*, 14840−14852. (e) Yamamoto, T.; Fukushima, T.; Kosaka, A.; Jin, W.; Yamamoto, Y.; Ishii, N.; Aida, T. *Angew. Chem., Int. Ed.* **2008**, *47*, 1672−1675. (f) Li, C.-H.; Chang, K.-C.; Tsou, C.-C.; Lan, Y.; Yang, H.-C.; Sun, S.-S. *J. Org. Chem.* **2011**, *76*, 5524−5530. (g) Maria, F. D.; Olivelli, P.; Gazzano, M.; Zanelli, A.; Biasiucci, M.; Gigli, G.; Gentili, D.; D'Angelo, P.; Cavallini, M.; Barbarella, G. *J. Am. Chem. Soc.* **2011**, *133*, 8654−8661.

(9) (a) Yang, W.-Y.; Lee, E.; Lee, M. *J. Am. Chem. Soc.* **2006**, *128*, 3484−3485. (b) Ajayaghosh, A.; Varghese, R.; George, S. J.; Vijayakumar, C. *Angew. Chem., Int. Ed.* **2006**, *45*, 1141−1144.

(10) (a) Wu, D.; Zhi, L.; Bodwell, G. J.; Cui, G.; Tsao, N.; Müllen, K. *Angew. Chem., Int. Ed.* **2007**, *46*, 5417−5420. (b) Shiomi, D.; Kanzaki, Y.; Okada, S.; Arima, R.; Miyazaki, Y.; Inaba, A.; Tanaka, R.; Sato, K.; Takui, T. *J. Phys. Chem. Lett.* **2011**, *2*, 3036−3039.

(11) (a) Panda, M.; Chandrasekhar, J. *J. Am. Chem. Soc.* **1998**, *120*, 13517−13518. (b) Yan, Y.; Yu, Z.; Huang, Y. W.; Yuan, W. X.; Wei, Z. X. *Adv. Mater.* **2007**, *19*, 3353−3357. (c) Suda, K.; Akagi, K. *Macromolecules* **2011**, *44*, 9473−9488. (d) Szostak, M. M.; Chojnacki, H.; Piela, K.; Okwieka-Lupa, U.; Bidzińska, E.; Dyrek, K. *J. Phys. Chem. A* **2011**, *115*, 7448−7455. (e) Sawada, Y.; Furumi, S.; Takai, A.; Takeuchi, M.; Noguchi, K.; Tanaka, K. *J. Am. Chem. Soc.* **2012**, *134*, 4080−4083. (f) Watanabe, K.; Osaka, I.; Yorozuya, S.; Akagi, K. *Chem. Mater.* **2012**, *24*, 1011−1024.

(12) (a) Hu, J.; Odom, T. W.; Lieber, C. M. *Acc. Chem. Res.* **1999**, *32*, 435−445. (b) Dai, H. *Acc. Chem. Res.* **2002**, *35*, 1035−1044. (c) Ouyang, M.; Huang, J.-L.; Lieber, C. M. *Acc. Chem. Res.* **2002**, *35*, 1018−1025. (d) Kamat, P. V. *J. Phys. Chem. C* **2007**, *111*, 2834−2860. (e) Lu, W.; Lieber, C. M. *Nat. Mater.* **2007**, *6*, 841−850. (f) Kamat, P. V. *J. Phys. Chem. C* **2008**, *112*, 18737−18753. (g) Hochbaum, A. I.; Yang, P. *Chem. Rev.* **2010**, *110*, 527−546. (h) Kamat, P. V. *J. Phys. Chem. Lett* **2010**, *1*, 520−527. (i) Lightcap, I. V.; Kamat, P. V. *Acc. Chem. Res.* **2013**, *46*, 2235−2243.

(13) (a) Iijima, S.; Ichihashi, T. *Nature* **1993**, *363*, 603−605. (b) Dresselhaus, M.; Dresselhaus, G.; Avouris, P. *Carbon Nanotubes: Synthesis, Properties, and Applications*; Springer-Verlag: Berlin, 2001. (c) Bachilo, S. M.; Strano, M. S.; Kittrell, C.; Hauge, R. H.; Smalley, R. E.; Weisman, R. B. *Science* **2002**, *298*, 2361−2366.

(14) (a) Weisman, R. B.; Bachilo, S. M. *Nano Lett.* **2003**, *3*, 1235−1238. (b) O'Connell, M. J. *Carbon Nanotubes Properties and Applications*; CRC Press: Boca Raton, 2006.

(15) (a) Tans, S. J.; Devoret, M. H.; Dai, H.; Thess, A.; Smalley, R. E.; Geerligs, L. J.; Dekker, C. *Nature* **1997**, *386*, 474−477. (b) Tans, S. J.; Verschueren, A. R. M.; Dekker, C. *Nature* **1998**, *393*, 49−52. (c) Choi, W. B.; Chung, D. S.; Kang, J. H.; Kim, H. Y.; Jin, Y. W.; Han, I. T.; Lee, Y. H.; Jung, J. E.; Lee, N. S.; Park, G. S.; Kim, J. M. *Appl. Phys. Lett.* **1999**, *75*, 3129−3131. (d) O'Connell, M. J.; Bachilo, S. M.; Huffman, C. B.; Moore, V. C.; Strano, M. S.; Haroz, E. H.; Rialon, K. L.; Boul, P. J.; Noon, W. H.; Kittrell, C.; Ma, J.; Hauge, R. H.; Weisman, R. B.; Smalley, R. E. *Science* **2002**, *297*, 593−596. (e) Misewich, J. A.; Martel, R.; Avouris, P.; Tsang, J. C.; Heinze, S.; Tersoff, J. *Science* **2003**, *300*, 783−786.

(16) (a) Zheng, M.; Jagota, A.; Semke, E. D.; Diner, B. A.; McLean, R. S.; Lustig, S. R.; Richardson, R. E.; Tassi, N. G. *Nat. Mater.* **2003**, *2*, 338−342. (b) Cathcart, H.; Nicolosi, V.; Hughes, J. M.; Blau, W. J.; Kelly, J. M.; Quinn, S. J.; Coleman, J. N. *J. Am. Chem. Soc.* **2008**, *130*, 12734−12744.

(17) Numata, M.; Asai, M.; Kaneko, K.; Bae, A.-H.; Hasegawa, T.; Sakurai, K.; Shinkai, S. *J. Am. Chem. Soc.* **2005**, *127*, 5875−5884.

(18) Dukovic, G.; Balaz, M.; Doak, P.; Berova, N. D.; Zheng, M.; Mclean, R. S.; Brus, L. E. *J. Am. Chem. Soc.* **2006**, *128*, 9004−9005.

(19) Zheng, M.; Jagota, A.; Strano, M. S.; Santos, A. P.; Barone, P.; Chou, S. G.; Diner, B. A.; Dresselhaus, M. S.; McLean, R. S.; Onoa, G. B.; Samsonidze, G. G.; Semke, E. D.; Usrey, M.; Walls, D. J. *Science* **2003**, *302*, 1545−1548.

(20) (a) Kang, Y. K.; Lee, O.-S.; Deria, P.; Kim, S. H.; Park, T.-H.; Bonnell, D. A.; Saven, J. G.; Therien, M. J. *Nano Lett.* **2009**, *9*, 1414−1418. (b) Deria, P.; Sinks, L. E.; Park, T.-H.; Tomezsko, D. M.;

Brukman, M. J.; Bonnell, D. A.; Therien, M. J. *Nano Lett.* **2010**, *10*, 4192−4199.
(21) (a) Park, J.; Deria, P.; Therien, M. J. *J. Am. Chem. Soc.* **2011**, *133*, 17156−17159. (b) Rosario-Canales, M. R.; Deria, P.; Therien, M. J.; Santiago-Avilés, J. J. *ACS Appl. Mater. Interfaces* **2012**, *4*, 102−109. (c) Larsen, B. A.; Deria, P.; Holt, J. M.; Stanton, I. N.; Heben, M. J.; Therien, M. J.; Blackburn, J. L. *J. Am. Chem. Soc.* **2012**, *134*, 12485−12491. (d) Bonhommeau, S.; Deria, P.; Glesner, M. G.; Talaga, D.; Najjar, S.; Belin, C.; Auneau, L.; Trainini, S.; Therien, M. J.; Rodriguez, V. *J. Phys. Chem. C* **2013**, *117*, 14840−14849.
(22) Frisch, M. J.; Trucks, G. W.; Schlegel, H. B.; Scuseria, G. E.; Robb, M. A.; Cheeseman, J. R.; Scalmani, G.; Barone, V.; Mennucci, B.; Petersson, G. A.; Nakatsuji, H.; Caricato, M.; Li, X.; Hratchian, H. P.; Izmaylov, A. F.; Bloino, J.; Zheng, G.; Sonnenberg, J. L.; Hada, M.; Ehara, M.; Toyota, K.; Fukuda, R.; Hasegawa, J.; Ishida, M.; Nakajima, T.; Honda, Y.; Kitao, O.; Nakai, H.; Vreven, T.; Montgomery, J., J. A.; Peralta, J. E.; Ogliaro, F.; Bearpark, M.; Heyd, J. J.; Brothers, E.; Kudin, K. N.; Staroverov, V. N.; Kobayashi, R.; Normand, J.; Raghavachari, K.; Rendell, A.; Burant, J. C.; Iyengar, S. S.; Tomasi, J.; Cossi, M.; Rega, N.; Millam, J. M.; Klene, M.; Knox, J. E.; Cross, J. B.; Bakken, V.; Adamo, C.; Jaramillo, J.; Gomperts, R.; Stratmann, R. E.; Yazyev, O.; Austin, A. J.; Cammi, R.; Pomelli, C.; Ochterski, J. W.; Martin, R. L.; Morokuma, K.; Zakrzewski, V. G.; Voth, G. A.; Salvador, P.; Dannenberg, J. J.; Dapprich, S.; Daniels, A. D.; Farkas, Ö.; Foresman, J. B.; Ortiz, J. V.; Cioslowski, J.; Fox, D. J. *Gaussian 09*; Revision A.1; Gaussian Inc.: Wallingford CT, 2009.
(23) (a) Stephens, P. J.; McCann, D. M.; Butkus, E.; Stončius, S.; Cheeseman, J. R.; Frisch, M. J. *J. Org. Chem.* **2004**, *69*, 1948−1958. (b) McCann, D. M.; Stephens, P. J. *J. Org. Chem.* **2006**, *71*, 6074−6098. (c) Mayer, Z. A.; Kállay, M.; Kubinyi, M.; Keglevich, G.; Ujj, V.; Fogassy, E. *J. Mol. Struct.: THEOCHEM* **2009**, *906*, 94−99. (d) Stephens, P. J.; Harada, N. *Chirality* **2010**, *22*, 229−233.
(24) O'Boyle, N. M.; Tenderholt, A. L.; Langner, K. M. *J. Comput. Chem.* **2008**, *29*, 839−845.
(25) Phillips, J. C.; Braun, R.; Wang, W.; Gumbart, J.; Tajkhorshid, E.; Villa, E.; Chipot, C.; Skeel, R. D.; Kalé, L.; Schulten, K. *J. Comput. Chem.* **2005**, *26*, 1781−1802.
(26) (a) Spellmeyer, D. C.; Grootenhuis, P. D. J.; Miller, M. D.; Kuyper, L. F.; Kollman, P. A. *J. Phys. Chem.* **1990**, *94*, 4483−4491. (b) Lee, O.-S.; Saven, J. G. *J. Phys. Chem. B* **2004**, *108*, 11988−11994. (c) Lee, H.; Venable, R. M.; MacKerell, A. D., Jr.; Pastor, R. W. *Biophys. J.* **2008**, *95*, 1590−1599.
(27) Johnson, R. R.; Johnson, A. T. C.; Klein, M. L. *Nano Lett.* **2008**, *8*, 69−75.
(28) Albertorio, F.; Hughes, M. E.; Golovchenko, J. A.; Branton, D. *Nanotechnology* **2009**, *20*, No. 395101.
(29) Ogawa, K.; Chemburu, S.; Lopez, G. P.; Whitten, D. G.; Schanze, K. S. *Langmuir* **2007**, *23*, 4541−4548.
(30) Chen, Y.; Liu, H.; Ye, T.; Kim, J.; Mao, C. D. *J. Am. Chem. Soc.* **2007**, *129*, 8696−8697.
(31) (a) Zheng, M.; Diner, B. A. *J. Am. Chem. Soc.* **2004**, *126*, 15490−15494. (b) Campbell, J. F.; Tessmer, I.; Thorp, H. H.; Erie, D. A. *J. Am. Chem. Soc.* **2008**, *130*, 10648−10655. (c) Campbell, J. F.; Napier, M. E.; Feldberg, S. W.; Thorp, H. H. *J. Phys. Chem. B* **2010**, *114*, 8861−8870.
(32) (a) Colter, A. K.; Clemens, L. M. *J. Phys. Chem.* **1964**, *68*, 651−654. (b) Kranz, M.; Clark, T.; Schleyer, P. v. R. *J. Org. Chem.* **1993**, *58*, 3317−3325. (c) Sahnoun, R.; Koseki, S.; Fujimura, Y. *J. Mol. Struct.* **2005**, *735*, 315−324.
(33) Olivier, J.-H.; Deria, P.; Park, J.; Kumbhar, A.; Andrian-Albescu, M.; Therien, M. J. *Angew. Chem., Int. Ed.* **2013**, DOI: 10.1002/anie.201307256.
(34) Jorgensen, W. L.; Chandrasekhar, J.; Madura, J. D.; Impey, R. W.; Klein, M. L. *J. Chem. Phys.* **1983**, *79*, 926−935.
(35) Von Bargen, C. D.; MacDermaid, C. M.; Lee, O.-S.; Deria, P.; Therien, M. J.; Saven, J. G. *J. Phys. Chem. B* **2013**, DOI: 10.1021/jp402140t.
(36) (a) Lin, V. S.; DiMagno, S. G.; Therien, M. J. *Science* **1994**, *264*, 1105−1111. (b) Lin, V. S.-Y.; Therien, M. J. *Chem.—Eur. J.* **1995**, *1*, 645−651. (c) Kumble, R.; Palese, S.; Lin, V. S.-Y.; Therien, M. J.; Hochstrasser, R. M. *J. Am. Chem. Soc.* **1998**, *120*, 11489−11498. (d) Shediac, R.; Gray, M. H. B.; Uyeda, H. T.; Johnson, R. C.; Hupp, J. T.; Angiolillo, P. J.; Therien, M. J. *J. Am. Chem. Soc.* **2000**, *122*, 7017−7033. (e) Fletcher, J. T.; Therien, M. J. *Inorg. Chem.* **2002**, *41*, 331−341. (f) Susumu, K.; Therien, M. J. *J. Am. Chem. Soc.* **2002**, *124*, 8550−8552. (g) Rubtsov, I. V.; Susumu, K.; Rubtsov, G. I.; Therien, M. J. *J. Am. Chem. Soc.* **2003**, *125*, 2687−2696. (h) Duncan, T. V.; Susumu, K.; Sinks, L. E.; Therien, M. J. *J. Am. Chem. Soc.* **2006**, *128*, 9000−9001. (i) Duncan, T. V.; Wu, S. P.; Therien, M. J. *J. Am. Chem. Soc.* **2006**, *128*, 10423−10435. (j) Susumu, K.; Frail, P. R.; Angiolillo, P. J.; Therien, M. J. *J. Am. Chem. Soc.* **2006**, *128*, 8380−8381. (k) Frail, P. R.; Susumu, K.; Huynh, M.; Fong, J.; Kikkawa, J. M.; Therien, M. J. *Chem. Mater.* **2007**, *19*, 6062−6064. (l) Banerjee, P.; Conklin, D.; Nanayakkara, S.; Park, T.-H.; Therien, M. J.; Bonnell, D. A. *ACS Nano* **2010**, *4*, 1019−1025. (m) Duncan, T. V.; Frail, P. R.; Miloradovic, I. M.; Therien, M. J. *J. Phys. Chem. B* **2010**, *114*, 14696−14702. (n) Conklin, D.; Nanayakkara, S.; Park, T.-H.; Lagadec, M. F.; Stecher, J. T.; Therien, M. J.; Bonnell, D. A. *Nano Lett.* **2012**, *12*, 2414−2419. (o) Li, Z.; Park, T.-H.; Rawson, J.; Therien, M. J.; Borguet, E. *Nano Lett.* **2012**, *12*, 2722−2727. (p) Conklin, D.; Nanayakkara, S.; Park, T.-H.; Lagadec, M. F.; Stecher, J. T.; Chen, X.; Therien, M. J.; Bonnell, D. A. *ACS Nano* **2013**, *7*, 4479−4486.
(37) Paolucci, D.; Franco, M. M.; Iurlo, M.; Marcaccio, M.; Prato, M.; Zerbetto, F.; Pénicaud, A.; Paolucci, F. *J. Am. Chem. Soc.* **2008**, *130*, 7393−7399.
(38) Sprafke, J. K.; Stranks, S. D.; Warner, J. H.; Nicholas, R. J.; Anderson, H. L. *Angew. Chem., Int. Ed.* **2011**, *50*, 2313−2316.